NILU: TR 1/2000

NILU: TR 1/2000
REFERENCE: U-95091/U-98009
DATE: JANUARY 2000
ISBN: 82-425-1150-0

The development of the SYMOCS instruments and the spectral analysis

Kjersti K. Tørnkvist

Contents

Abstract

Since 1995, Norwegian Institute for Air Research (NILU) has measured the stratospheric compounds O_3, NO_2, BrO and OClO with a ground-based spectrometer that measures the scattered light from the zenith sky. The instrument system called SYMOCS (SYstem for MOnitoring Compounds in the Stratosphere), was developed at NILU and measured from Ny-Ålesund (Spitsbergen) from autumn 1995. During the autumn 1996 the instrument measured from Longyearbyen, but continued to measure from Ny-Ålesund throughout spring 1997. During 1998 a similar spectrometer system was developed in order to optimise the measurements of the four compounds. The two instrument systems are called SYMOCS-VIS (O_3 and NO_2) and SYMOCS-UV (BrO and OClO). This report describes the development and the characterisation of the two instruments. The measured spectra are analysed with the well established method called DOAS (Differential Optical Absorption Spectroscopy). A proper analysis and retrieval of the compounds requires a optimised set of analysis parameters. The principles behind the analysis and the analysis parameters are described in detail in the second part of this report.

The development of the SYMOCS instruments and the spectral analysis

1 Introduction

Over the last decades, significant ozone depletion has taken place during winter and early spring in the Arctic region (e.g. European Commission, 1997; United Kingdom Stratospheric Ozone Review Group, 1999). It has been clearly demonstrated that chlorine and bromine compounds lead to chemical destruction of stratospheric ozone, and that their presence could account quantitatively for the formation of the ozone hole. The increase in the chlorine and bromine amounts in the stratosphere is mainly due to anthropogenic release of CFC compounds. NO_2, ClO and BrO are three of the most important species involved in catalytic ozone depletion. The underlying chemistry is not a topic of this report, but details can be found elsewhere (e.g. Wayne, 1991; Solomon, 1999).

UV-visible spectroscopy is a useful technique for investigating ozone and the mechanisms to its depletion. The Norwegian Institute for Air Research (NILU) decided in 1994 to develop a ground-based UV-visible spectrometer for measurements of compounds in the stratosphere. The aim was to build up further competence for measurement and retrieval of stratospheric compounds. NILU already operated a SAOZ[1] instrument (Høiskar, 1997), but this instrument only measures O_3 and NO_2. The purpose of the new spectrometer system was to include measurements of the halogen trace gases BrO and OClO. With this instrument, the four trace gases O_3, NO_2, BrO and OClO are measured in the same airmass, enabling interpretation of the *in situ* chemistry. During the course of this work, the need for two systems (one for measuring O_3 and NO_2, and the other for measuring BrO and OClO) and the optimisation of the measurements of each trace gas arose.

The first spectrometer system was called SYMOCS (SYstem for MOnitoring Compounds in the Stratosphere). It was first installed at Ny-Ålesund/Spitsbergen (79°N, 11°E) autumn 1995. During the autumn 1996 the instrument measured from Longyearbyen, but continued to measure from Ny-Ålesund through spring 1997. During this period (1995-1997), all four compounds were measured by one spectrometer system. This instrument participated in an intercomparison campaign at Observatorie Haute de Provence (OHP, 43.9°N, 5.7°E) in June 1996 (Roscoe et al., 1999 and Aliwell et al., 2000). Some of the results obtained during the campaign and workshop are described in this report (Chapter 3).

During 1998, the second spectrometer system, SYMOCS-UV, was developed. The two systems were after this called SYMOCS-VIS and SYMOCS-UV, where SYMOCS-VIS is configured to measured O_3 and NO_2 and SYMOCS-UV measures BrO and OClO. Both systems are now in operation at the Andøya

[1] System for Analysis of Observations and Zenith; DOAS-instrument developed by J.-P. Pommereau and F. Goutail (CNRS, France)

Rocket Range (69.3°N, 16°E). A more thorough discussion of the performance of the instruments is given in Tørnkvist (2000).

This report consists of two main parts. Chapter 2 describes the development of the two ground-based UV-visible spectrometer systems as well as a description and characterisation of the instruments. Chapter 3 focuses on the analysis procedure which is the well known DOAS-technique (Differential Optical Absorption Spectroscopy) first developed by Platt et al. (1979) for tropospheric trace gas studies. The method has been proven to be a useful tool for the retrieval of slant columns of several atmospheric trace gases. In this work, the method is applied to spectra measured viewing the zenith sky. Furthermore, all important parameters and effects that have to be taken into account when analysing zenith sky spectra are described, ending in a summary describing the parameter sets that have been found to be optimal for the analysis of the four gas compounds from the SYMOCS' spectra. These parameter sets are based on the currently available absorption cross sections.

2 Development of Zenith-Sky Spectrometers to measure O_3, NO_2, OClO and BrO

2.1 Basic considerations

UV-visible absorption spectroscopy is a technique that has been proven to be very useful for simultaneous monitoring of slant columns of atmospheric trace gases such as O_3, NO_2, OClO and BrO (Solomon et al., 1987; Hofmann et al. 1995; Vaughan et al. 1997; Roscoe et al., 1999). Two spectrometers measuring the absorption of scattered light from the zenith sky have been developed. The spectrometers consist of a commercial monochromator and a 1024 photodiode array detector and measure atmospheric spectra in the ultraviolet (UV) and in the visible wavelength region (330-550 nm). The spectra are then analysed to retrieve differential slant columns of the atmospheric trace gases that absorb in the measured wavelength interval.

When spectra are measured using an array detector of limited size and number of pixels, there is always a trade-off between the different instrumental parameters such as

- the wavelength interval that can be covered, which in turn limits the number of different atmospheric species that can be measured simultaneously,
- the instrumental resolution and the sampling ratio, and
- the through-put or signal strength which is proportional to the width of the entrance slit.

The instrument parameters have to be optimised for the different measurement conditions. The wavelength interval that is covered increases with decreasing focal length (f) and decreasing number of lines in the grating (n). The instrumental resolution, ($\Delta\lambda$), however, gets poorer when the focal length and n is decreased. $\Delta\lambda$ is also dependent on the width of the entrance slit (d) through the following relationship

$$\Delta\lambda \propto \frac{d}{f} \cdot \frac{1}{n} \qquad \textit{Eq. 2.1}$$

Increasing the entrance slit width results in a poorer resolution, but the sampling ratio or the oversampling, will increase. The sampling ratio of a spectral line, which is the number of detector pixels covering the full width at half maximum (FWHM) of the instrument resolution function, is a very important parameter. According to the Nyquist theorem, at least two points per period of the maximum frequency are needed to measure the absorption features in a spectrum properly. When a spectrum measured at a finite resolution is recorded with insufficient points to represent its true shape, we get a condition known as undersampling. A necessary part of the retrieval algorithm used in this work require the ratio of a pair of spectra to be determined (Chap. 3.2). If their wavelength calibration differ and if an array detector is used, at least one spectrum must be interpolated. The interpolation process introduces errors if the spectrum is undersampled (Roscoe et al., 1996).

The systems consist of several units, which are described in the following sections. These are the spectrograph with a grating controller (Chap. 2.2), the photodiode array detector with a detector controller and cooler (Chap. 2.3), a fibre and a computer to run the system automatically. A schematic layout of the ground-based SYMOCS instruments is shown in Figure 2.1, and an example of a measured zenith sky spectrum for the 330-480 nm wavelength interval is displayed in Figure 2.2. The spectrum is recorded under clear sky conditions at 90° SZA (AM) on 3 March 1996 at Ny-Ålesund.

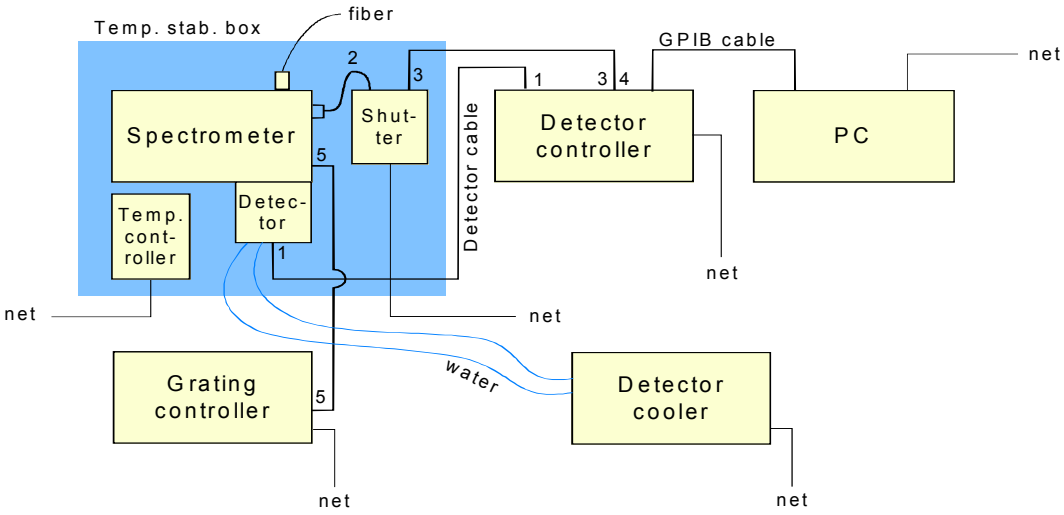

Figure 2.1: Schematic layout of the SYMOCS instruments developed at the Norwegian Institute for Air Research.

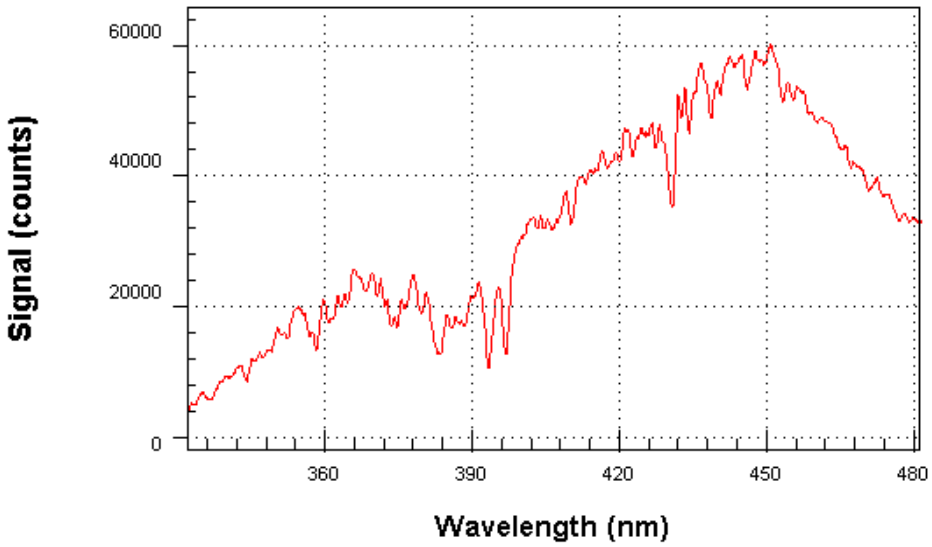

Figure 2.2: The zenith sky spectrum for the 330-480 nm wavelength interval measured under clear sky conditions 3 March 1996 at Ny-Ålesund at 90° SZA (AM).

2.2 The Spectrometer

Both zenith-sky instruments consist of a SpectraPro-275 triple grating spectrograph from Acton Research Corporation with a focal length of 275 mm. The spectrograph is equipped with three plane gratings mounted on a turret controlled by a stepper motor and two concave mirrors in a Czerny-Turner arrangement. However, the grating position is always fixed for our measurements (see Chapter 2.3). The spectrometer has a flat 25 mm wide focal plane. The optical layout of the Czerny-Turner spectrometer is shown in Figure 2.3.

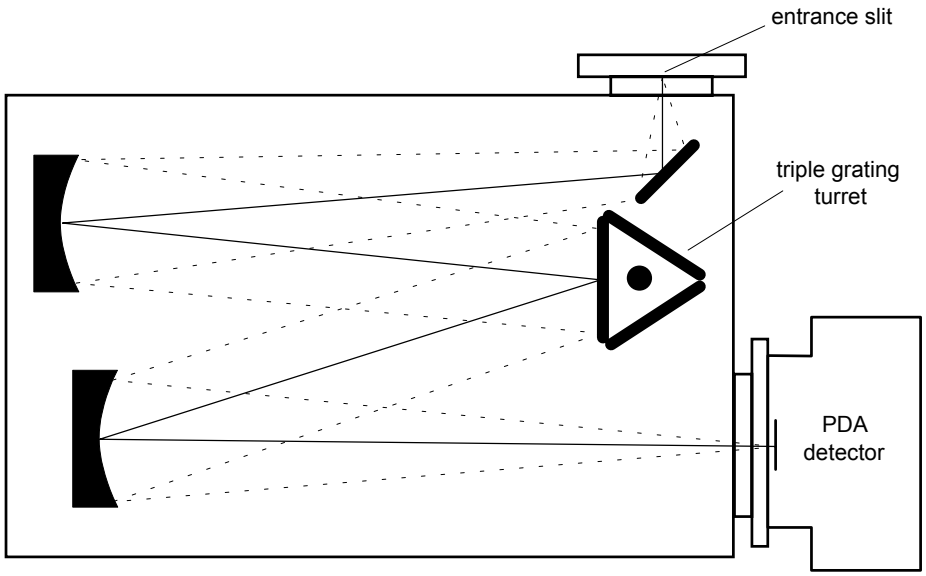

Figure 2.3: The optical layout of the Acton SpectraPro-275 monochromator.

The dimensions of the plane, ruled gratings are 68x84 mm which gives an aperture ratio of f/3.2. The spectral range covered depends on the focal length and the grating. The relation between spectral range and grating chosen for a spectrometer with a focal length of 275 mm is given in Table 2.1.

Table 2.1: Spectral range covered using different gratings (fixed focal length of 275 mm).

Grating type	600 g/mm	1200 g/mm	2400 g/mm
Spectral range	150 nm	75 nm	37.5 nm

For the measurements at Ny-Ålesund with the first system, the 600 g/mm grating was chosen to be able to detect all the four compounds of interest (O_3, NO_2, BrO and OClO). The wavelength interval was 332-482 nm. The width of the entrance slit, which is one of the parameters that determines the spectral resolution, is adjustable over a range from 10 µm to 3.0 mm via an external micrometer screw. The entrance slit width for the measurements at Ny-Ålesund was 150 µm, resulting in a spectral resolution of approximately 0.9 nm FWHM and a sampling ratio of approximately 6.

Scattered light from the zenith sky is collected by an optical quartz fibre with a 200 µm x 2.5 mm slit converter coupled directly to the entrance slit through a mechanical fibre adapter. The field of view is 18° (full angle).

2.3 The Photodiode Array Detector

Both instruments are equipped with a photodiode array detector to simultaneously measure the entire wavelength range. This is in contrast to a conventional spectrograph where the spectral elements are observed sequentially for short periods. A consequence of this could be that all spectral elements are not necessarily observed under the same light conditions e.g. due to change in cloud coverage under the total measurement time. An additional advantage using diode array is avoiding a rotation of the grating which results in an improved stability of the wavelength axis. A brief explanation of how the photodiode array works is given in the following.

A reverse voltage charges each diode. Illumination of the diode causes electron-hole pair recombination, which reduces the charge of the diode. The reduction is a function of the intensity of the incoming light and the exposure time of the measurement. The analogue signal from each diode is the removed charge. The signal from all diodes is read sequentially before the diodes again are recharged for the next measurement. The analogue signal is amplified in the detector head before it is sent to the controller for further processing and digitising.

Electrons in the valence band can also be thermally excited causing a leakage of the diode charge. This is called the dark current of the photodiode array. The dark current decreases as the temperature of the detector array is reduced, typically a factor of two for every 7°C reduction. To minimise the dark current, it is very important to cool the detector as much as possible. In this case, the detectors are

cooled to -40ºC. The diode array is seated on a cold finger which itself is seated on a two-stage Peltier cooler. The temperature difference from the warm and the cold side of the Peltier element can be -40°C. To remove the heat from the thermoelectrical cooler, a water coolant at about 5°C is circulated through the back-plate of the detector. An indication lamp on the detector controller gives information about the temperature status. The accuracy of the thermostat is ±0.05°C of the set temperature. The external cooler is a Neslab RTE100. The chamber where the detector head is seated is evacuated through a vacuum valve to prevent internal condensation. The detector has to be evacuated approximately every third month.

Before analysing an atmospheric spectrum, the dark current contribution to the signal has to be subtracted from the measured spectrum. An accurate knowledge of the dark current is therefore important. The dark current varies from one detector to the other and from one individual diode to another. Figure 2.4 (upper panel) displays a dark current spectrum from the detector with the Hamamatsu chip measured the 3 March 1996 with an integration time of 300 s. In the lower panel a dark current spectrum from the Reticon detector is shown for identical measurement conditions. Each detector's own particular set of dark current spectra is measured every day for all used exposure times. The appropriate dark current spectrum is found and subtracted from each measured atmospheric spectrum.

A photodiode array detector consisting of 1024 independent silicon diodes (often called pixels) from Princeton Instruments, was mounted on the first spectrometer (RY-1024/H diode array detector). A detector-chip from Hamamatsu was chosen because the dark current is known to be very low. The pixel size was 24.9 μm x 2.5 mm. Unfortunately this detector had to be replaced with a Reticon 1024 diode array detector (Princeton Instruments Inc.) in 1998 in the SYMOCS-VIS instrument when the Hamamatsu detector broke down, and a replacement was not available. A similar Reticon detector was installed in the SYMOCS-UV. Two significant differences between the Hamamatsu detector and the Reticon are that (i) the dark current is higher for the Reticon detector and (ii) the handling of the odd and even diodes which are on separate circuits in the Reticon detector. The gain of both preamplifiers (odd and even) has to be carefully equalised to achieve optimal baseline uniformity. Both pattern and dark current are temperature dependent.

The so-called etaloning structures in the recorded spectra (Mount et al., 1992) caused by the passivated silicon layer on top of the detector chip is a well known problem with photodiode detectors. This can be avoided by mounting a wedged window in front of the detector head. A wedged window was mounted on the Hamamatsu detector and on the detector of the SYMOCS-UV. Unfortunately this was not possible for the new SYMOCS-VIS detector. However, no etaloning structure has been observed.

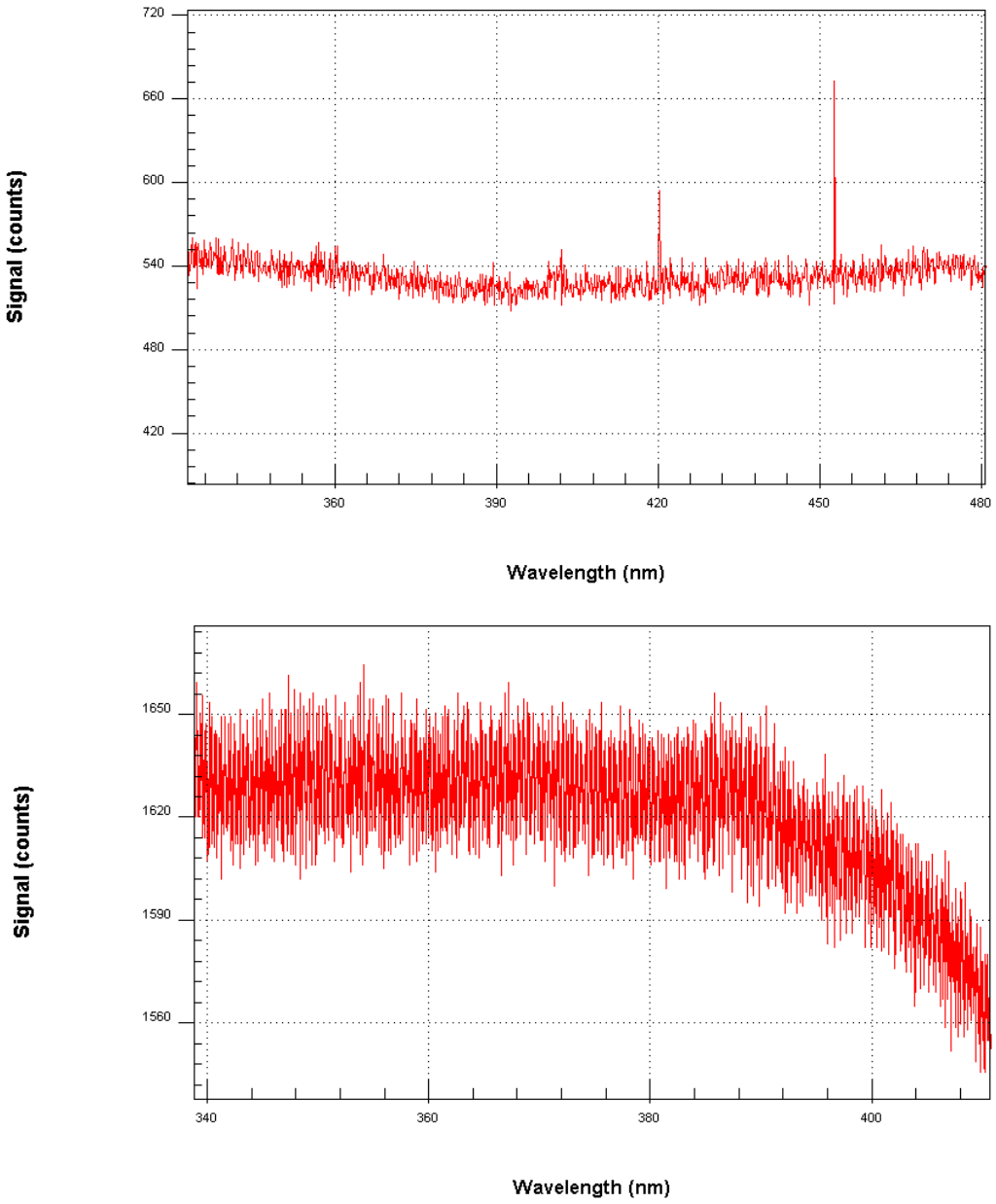

Figure 2.4: Dark current spectra from two different photodiode array detectors under identical measurement conditions (300 s integration time). In the upper panel the dark current detector with a Hamamatsu chip is shown (3 March 1996), and in the lower panel the dark current from the Reticon detector is shown (3 March 1999).

2.4 Stray Light Performance of the Spectrometer

An ideal spectrometer has no stray light. Light at each wavelength reaches a specific place on the exit focal plane. Stray light is defined as light other than the wavelength of interest that reaches a detector pixel, and stray light in the spectrometer can represent a serious problem. Stray light gives an additional signal on top of the true signal on the pixels.

Common sources of stray light are:

- light of unused diffraction orders reflected from the interior walls,
- light scattered from the internal optical elements (grating and mirrors) due to overfilled optical elements or due to scratches on the surface, and
- reflections from the detector surface back into the spectrometer.

To avoid overfilled optical elements one can use baffling, and to avoid reflection from the diode array one can for example tilt the array, but not so much that the resolution is degraded. In both systems described here, the array is tilted.

The amount of stray light in the Acton SpectraPro-275 was characterised by using long-pass filters to measure stray light from wavelengths longer than the filter cut-off. A Schott filter (GG495 nm) was used in the tests. This filter cuts off light above approximately at 495 nm. A spectrum measured with the filter should consist of only stray light, while a spectrum measured without the filter is a combination of the 'pure' spectrum and stray light. The ratio of these two spectra gives an estimate of the level of stray light in the measured spectra. For SYMOCS the stray light contribution to a spectrum was found to be approximately 1.2% in the visible region. A stray light contribution at this level can be corrected for in the analysis (Chap. 3.4).

2.5 Polarisation

A spectrograph may be sensitive to polarisation of the incoming light. Scattered sky light is generally partly polarised, and a spectrograph that is sensitive to polarisation will produce spectra containing features that vary with solar zenith angle and solar azimuth angle. It is therefore advantageous to use a spectrometer system that is insensitive to polarisation. A fibre bundle depolarises light, and tests performed on the polarisation sensitivity of the SYMOCS instruments showed that they are sufficiently insensitive to polarisation not to introduce significant errors. In Figure 2.5 the ratio of the $|\vec{E}|$-parallel and the $|\vec{E}|$-perpendicular to the entrance slit (polarisation ratio) is shown. The $\vec{E}$ is the electric field in the light. The ratio, *R*, is almost independent of wavelength, indicating that the systems show no polarisation sensitivity as function of wavelength. The structures around 395 nm and 432 nm are due to a not completely removal of the strong Fraunhofer lines when the ratio of the two spectra were calculated.

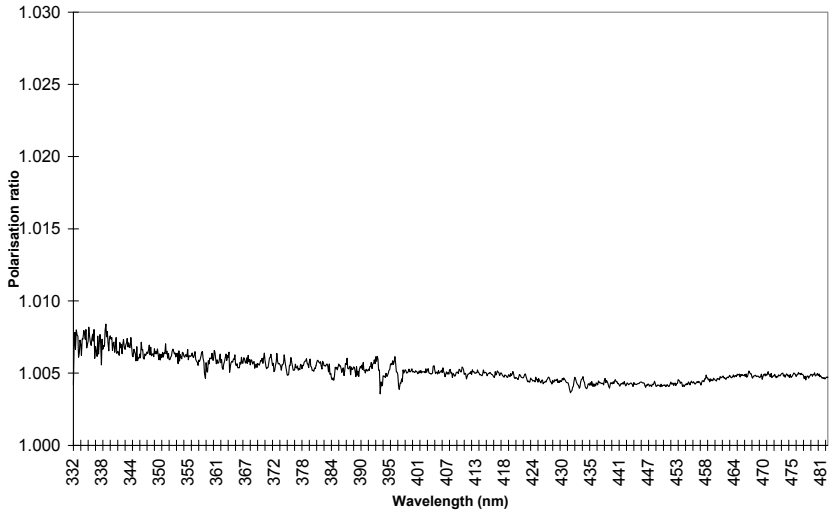

Figure 2.5: The ratio of the $|\vec{E}|$-parallel and the $|\vec{E}|$-perpendicular to the entrance slit for the SYMOCS-VIS instrument.

2.6 Detector Linearity and Dynamic Range

The dynamic range of the three detectors used in this work (one Hamamatsu detector and two Reticon detectors) was tested by two different methods:

1. Light from a halogen light source was directed into the spectrometer and the increase in signal as a function of the exposure time was measured,
2. The ratio between the signals at the pixel with maximum signal and at a pixel with lower signal was calculated.

As is seen in Figure 2.6, the Hamamatsu detector began to saturate around 48.000-52.000 counts. In the software for running the instrument, the integration time is therefore chosen such that the signal level does not exceed 48.000 counts, which is approximately 75% of maximum counts (65.000). The Reticon detector began to saturate around 50.000–55.000 counts, and maximum signal level is therefore chosen to 50.000 counts.

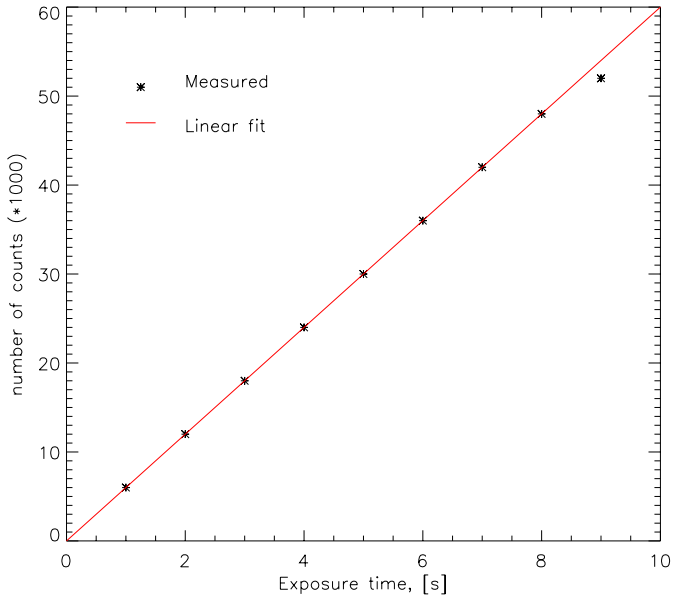

Figure 2.6: Number of counts from the Hamamatsu detector at constant incident light flux as function exposure time. In black are the measured results. The red line is a first order polynomial fitted to the measured data points. The last point is not included in the linear fit.

2.7 Instrument Line Shape Function and Wavelength Calibration

In this section, a description of the method for obtaining an accurate wavelength calibration and a characterisation of the instrument response is given. The spectral resolution and sampling ratio of the different instruments and configurations are briefly described together with the effect of the sampling ratio on the spectral analysis.

2.7.1 Wavelength Calibration

The relationship between the pixels of the detector and the corresponding wavelength of the spectrum has to be found. The emission lines in a Cadmium-Mercury lamp are used in an approximate wavelength calibration. The {pixel, CdHg-wavelength}-pairs are fitted by a second-degree polynomial by using a least square fit. The analysis software (Chapter 3.2.1) determines a more exact wavelength calibration by using the high resolution Fraunhofer reference spectrum measured by a Fourier transform Spectrometer (FTS) at Kitt Peak (Arizona, U.S.A.) (Kurucz et al., 1984). Calibration is achieved by matching the Fraunhofer absorption lines in the measured spectra to those in the high resolution Fraunhofer spectrum. This procedure is performed on the reference spectrum used in the analysis (Chapter 3.2), which is either a noon spectrum or a spectrum taken at a specified SZA. All other spectra and convoluted cross sections are shifted according to the calibrated reference spectrum.

2.7.2 Instrument Line Shape Function

The instrument line shape (ILS) function of an ideal spectrometer are a delta function. Due to the finite width of the entrance slit and of the detector pixels, the

finite size of the optical elements, aberration effects and the quality and alignment of the optical components, the spectrometer will always produce an apparent spectral broadening of the monochromatic light. The measured spectrum, $I_{meas}(\lambda)$, of an external light source is a convolution of the ILS function, $F(\lambda)$, and the real spectrum of the external light source, $I_{source}(\lambda)$

$$I_{meas}(\lambda) = (I_{source} * F)(\lambda) = \int_{-\infty}^{\infty} I_{source}(\lambda - \lambda')F(\lambda')d\lambda'. \qquad Eq.\ 2.2$$

An accurate determination of the ILS function is of vital importance in the DOAS analysis of the measured spectra (Chapter 3.2). The ILS function is necessary for the proper filtering of the absorption cross section reference spectra used in the retrieval process as well as for the high resolution Fraunhofer spectrum used in the wavelength calibration procedure.

The ILS function can be found by measuring the spectrum of a cadmium-mercury emission lamp. The ILS function may vary as a function of wavelength, grating position and detector pixel, and also from day to day. For the filtering procedure, an emission line within or nearby the wavelength region to be analysed should be chosen. In addition, it would be best to measure the ILS function every day. A system to handle this has not yet been implemented.

Figure 2.7 shows an example of the ILS function for SYMOCS-VIS when the spectrometer is properly aligned. The measured ILS function fits very well to a Gaussian function. However, different measurements of the ILS function have shown that the shape of the ILS function can change due to changes within the spectrometer (i.e. temperature fluctuations) or the fibre-spectrometer coupling. If an improper ILS function is used in the convolution process described above, will this result in to large residuals (see Figure 2.9). The Gaussian function is the exact line shape in the diffraction limit i.e. in the case of an infinitely thin entrance slit, but is also a good approximation for the ILS function when a thin entrance slit is used. When the spectrometer is operated with a large entrance slit so that the corresponding ILS function is sampled with many points, the ILS function can be well represented by a function that mathematically is described as a boxcar convolution of a Gaussian function (Van Roozendael, personal communication). In the following, such a function is called an integrated Gaussian function. This results in a ILS function that is broader on the top than a Gaussian function. The ILS function measured at Ny-Ålesund in March 1997, is shown together with a fitted Gaussian function in Figure 2.8, and it is illustrating that the measured ILS function is broader on the top compared to a Gaussian function. However, the measured ILS function fits nicely to an integrated Gaussian function.

Measurements of a Mercury or Cadmium absorption line at an unsuitable wavelength or with incorrect filling of the instrument field of view may cause a poorly represented ILS function. The WinDOAS program, described in Chapter 3.2.1, includes the possibility of determining the resolution and best fitted line shape as a function of wavelength, using the Fraunhofer features in the actual measured spectrum. The same high resolution Fraunhofer reference spectrum

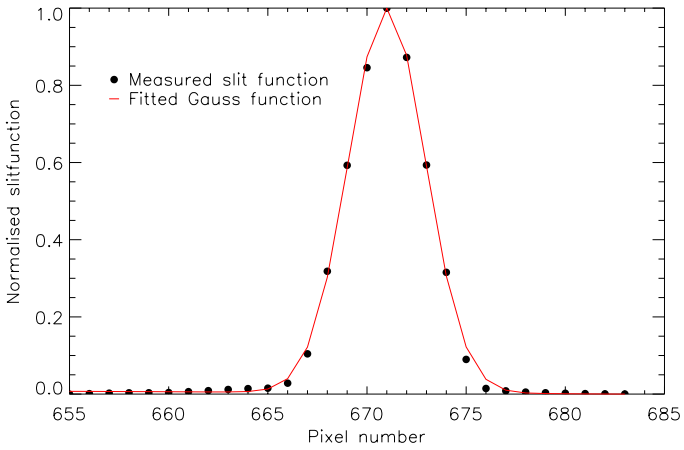

Figure 2.7: Instrument response function of SYMOCS-VIS at 435.8 nm measured May 1998 with the Cadmium-Mercury spectral lamp. The red curve is a Gaussian function fitted to the measured ILS function.

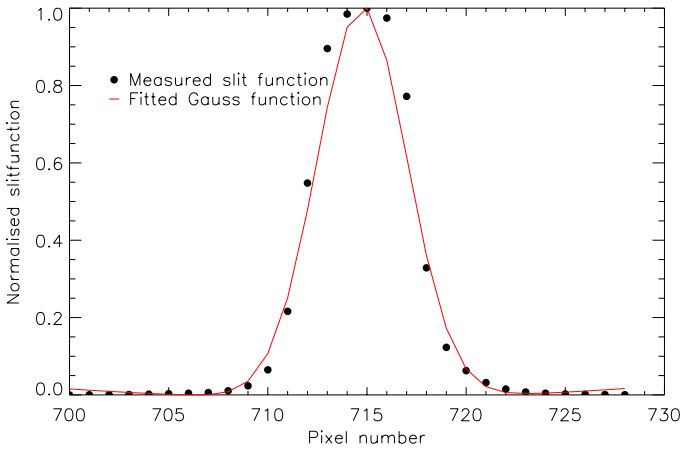

Figure 2.8: Instrument response function of SYMOCS-VIS at 435.8 nm measured March 1997 with a Mercury spectral lamp. The red curve is a Gaussian function fitted to the measured ILS function.

used for wavelength calibration (Kurucz et al., 1984), is convolved with a ILS function of wavelength dependent resolution to give the minimum residual between the measured spectrum and the convoluted Fraunhofer reference spectrum. Such a ILS function characterisation is performed on spectra measured by both SYMOCS-VIS and SYMOCS-UV. The residual between a measured spectrum and the convoluted Fraunhofer reference spectrum was significantly reduced when applying an integrated Gaussian ILS function compared to the measured ILS function or a Gaussian ILS function especially for the period at Ny-Ålesund and Longyearbyen (1995-1997). The residuals between a measured spectrum from 26 March 1996 and the convoluted Fraunhofer spectrum for the three mentioned cases are shown in Figure 2.9.

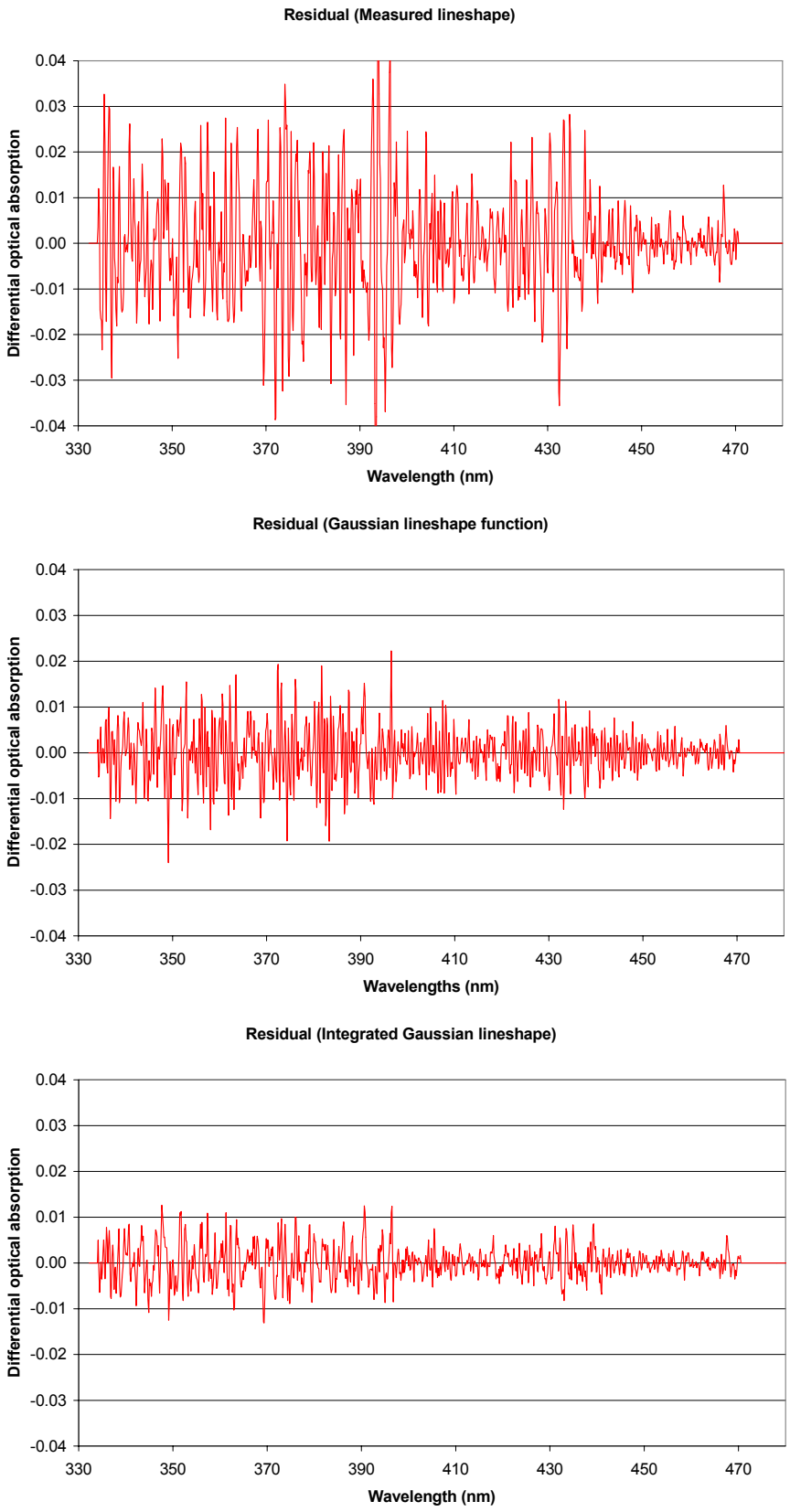

Figure 2.9: Residual between a measured spectrum from 26 March 1996 and the high resolution Fraunhofer reference spectrum when convolving with a ILS function of wavelength dependent resolution of type a) measured ILS function from 16 February 1996, b) Gaussian function and c) integrated Gaussian function.

A correct determination of the ILS function is very important for the retrieval of the atmospheric compounds. This is especially the case for BrO and OClO owing to their weak absorptions. When using the ILS function determined from the procedure described above, the retrieval of e.g. BrO is greatly improved. The fitting between the measured spectra and the cross section spectra and thereby the residuals are improved, and the retrieval errors decreased.

2.7.3 Spectral Resolution and Sampling Ratio

The spectral resolution is dependent on the focal length, the entrance slit-width and the grating (grooves/mm), and is found from the ILS function. The resolution may be wavelength dependent. The sampling ratio is the number of pixels covering the FWHM of the instrument resolution function. A higher sampling of the measured spectra leads to lower analysis errors in the retrieval (Hofmann et al., 1995). Noise in the ratio spectrum (see Chap. 3.2 for description of the DOAS analysis) is produced by the interpolation used to shift and stretch the twilight spectra onto the noon spectrum so that they are properly wavelength aligned with each other before the ratio spectrum is formed. Interpolation noise is reduced when a higher sampling ratio is used.

In the first spectrometer system, the entrance slit width was set to 150 μm. This, together with the focal length of 0.275 m and the grating of 600 grooves/mm, gives a spectral resolution of approximately 0.9 nm and a sampling ratio of approximately 6. This sampling ratio is sufficient for the measurements of O_3 and NO_2 since they are rather strong absorbers in the wavelength region chosen for their retrieval.

The sampling ratio was an important factor when designing the SYMOCS-UV spectrometer. The entrance slit width was increased to 200 μm and the grating used had 1200 grooves/mm, which gave a spectral resolution of approximately 0.6 nm and a sampling ratio of 10. The higher sampling ratio was chosen to improve the analysis of BrO and OClO by reducing the errors in the retrieval process. SYMOCS-VIS continued to have the same specifications as the first spectrometer system.

2.8 Temperature Regulation

A stable wavelength calibration is necessary in the retrieval process of the measured spectra. The calibration is highly dependent on the temperature in the spectrometer. A change in the temperature will change the position of the absorption lines on the detector array. To minimise this effect, the spectrometers were temperature stabilised in February 1996. Both spectrometers are installed in a temperature regulated insulated box which is temperature regulated to +40°C.

Originally, the temperature was set to +35°C. However, experience showed that the temperature in the room increased, primarily due to longer sunlight periods, so that it was difficult to stabilise the temperature to +35°C. The box temperature was therefore increased to +40°C on 30 March 1996. An increase in the spectrometer temperature of +5°C resulted in a spectral shift of ~0.55 nm which had to be adjusted for in the wavelength calibration. As mentioned in Chapter 2.7.3, large shifts and stretching to wavelength align the twilight spectra onto the background

spectrum, increases the retrieval error. Two different background spectra, one for the period before 30 March and one for the period afterwards, were found necessary to use to obtain the best possible results for the two periods. During the intercomparison campaign at OHP in June 1996, the temperature stabilisation did not work properly due to very high ambient air temperatures, especially in the afternoons.

2.9 Discussion of a New Spectrometer, SYMOCS-UV

As pointed out earlier, a sufficient oversampling together with a high spectral resolution is necessary in order to measure BrO. To be able to interpret the local chemistry, it is essential to measure all four trace gases O_3, NO_2, BrO and OClO in the same airmass. With only one spectrometer available, a compromise between resolution, oversampling and spectral range is apparent. Measurements of all compounds were possible when configuring the spectrometer such that the resolution was 0.9 nm and the oversampling was 6 pixel/FWHM. To get good measurements of BrO, it is preferable to have better resolution together with a higher sampling ratio. This came in conflict with the spectral range necessary to be able to measure all four compounds. An additional factor was that it is preferable to measure O_3 at higher wavelengths (480-550 nm) than possible with the configuration of the first SYMOCS spectrometer. Therefore it was decided to assemble a similar spectrometer system (SYMOCS-UV) to measure BrO and OClO, and use the old system (now SYMOCS-VIS) to measure O_3 and NO_2. SYMOCS-UV was assembled during spring 1998, and moved to the Andøya Rocket Range (ARR) in July 1998. SYMOCS-UV has a spectral resolution of 0.6 nm and an oversampling of 9 pixel/FWHM.

Another important advantage of using two instruments instead of one for measurement of the four compounds, is that the signal level in the UV-part of the spectrum will increase. This is due to the difference in intensity in the scattered zenith light in the two wavelength regions (330-400 nm and 330-480 nm). The maximum intensity in the atmospheric spectrum is around 450 nm (see Figure 2.2). To avoid saturation in the individual detector pixels, the exposure time is decided from the intensity of the pixel that detects the maximum signal. When measuring up to 480 nm, the signal around 450 nm determines the exposure time, and this signal is a factor 3-4 higher than at 350 nm. If only including wavelength up to 400 nm, the difference between maximum and minimum signal level is less. The exposure time and therefore the signal level for the UV-part of the spectrum can be increased by a factor of approximately 2. Figure 2.10 shows a zenith sky spectrum measured by the SYMOCS-UV instrument the 3 March 1999 at 90°SZA (AM).

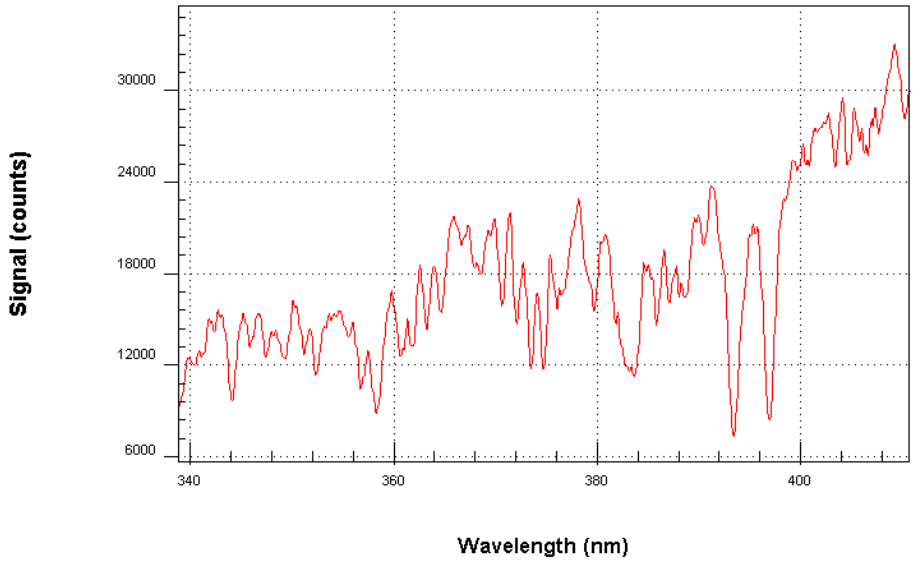

Figure 2.10: The zenith sky spectrum from 3 March 1999 (90°SZA, AM) measured from Andøya with the SYMOCS-UV instrument.

2.10 Measurement Periods and Instrumental Parameters

One of the aims of developing the SYMOCS spectrometers was to supplement NILU's SAOZ instrument at Ny-Ålesund which is a part of the NDSC[2] network.

The first SYMOCS system was initially installed at the NDSC building of the Alfred Wegener Institute for Polar and Marine Research (AWI) at Ny-Ålesund in the autumn 1995. The wavelength region for this particular autumn was set to 400-550 nm, and O_3 and NO_2 were retrieved from the spectra. Due to a problem with the electronic detector cooler within the detector controller, data collection started on 25 September (normally 20 August). The measurement period at Ny-Ålesund is limited to the period from the middle of February to the end of April and from late August to the end of October. This is because there is no sun during the polar winter and the sun is too high during the polar summer for reliable DOAS measurements. The measurement period at Andøya is restricted to the period between 17 January to 5 June, and between 10 July to 30 November. In Table 2.2 the different instrument configurations, measurement sites and time-periods for the spectrometer systems are given. As seen from the table, the first SYMOCS system has been installed at several measurement sites and in different configurations. SYMOCS-UV has only been operating at Andøya.

[2] Network for the Detection of Stratospheric Change

Table 2.2: The different configurations, measurement sites and time-periods for operation of SYMOCS-VIS and SYMOCS-UV.

Configurations of the SYMOCS-VIS spectrometer						
Time period	**Measurement site**	**Grating**	**Wavelength region**	**Entrance slit width**	**Wavelength calibration**	**Comments**
25.09.95-30.10.95	Ny-Ålesund, (78.9°N,11.9°E)	600 g/mm	400-550 nm	150 µm	Hg	• Spectrometer not temperature stabilised • Measurement started late in September due to problems with the cooling of the detector
17.02.96-27.04.96	Ny-Ålesund, (78.9°N,11.9°E)	600 g/mm	332-482 nm	150 µm	Hg	• Spectrometer is now temperature stabilised • **30.03.96 :** Changed temperature of spectrometer from +35°C to +40°C
11.06.96-27.06.96	OHP (43.9°N,5.7°E)	600 g/mm	332-482 nm	150 µm	Hg	• NDSC intercomparison campaign and SCUVS-3 workshop
20.08.96-30.10.96	Longyearbyen, (78.2°N,15.6E)	600 g/mm	332-482 nm	130 µm	Hg	
11.03.97-30.04.97	Ny-Ålesund, (78.9°N,11.9°E)	600 g/mm	332-482 nm	150 µm	Hg	
04.06.98-15.07.98	Andøya, (69.3°N,16.0°E)	600 g/mm	332-482 nm	150 µm	HgCd	• Installed GPS for time setting • **January-May 1998 :** Several problems with the detector controller and detector preamplifier, sent to Germany for repair • **18.06-24.06 :** Fibre not viewing the zenith sky • **July 1998-March 1999:** New problem with detector preamplifier, sent to Germany for repair
26.03.99-01.07.99			400-550 nm	150 µm	HgCd	• Detector broke down in July 1999, will be reinstalled in February 2000

Configurations of SYMOCS-UV						
Time period	**Measurement site**	**Grating**	**Wavelength region**	**Entrance slit width**	**Wavelength calibration**	**Comments**
15.07.98-	Andøya, (69.3°N,16.0°E)	1200 g/mm	339-410 nm	200 µm	HgCd	• GPS for time setting

2.11 Logging of Spectra and Measurement Routines

The instruments are controlled by a software package called SPEC-RUN, developed at NILU. The SPEC-RUN software controls the measurement parameters, collects the spectra, stores them, and controls the measurements of the dark current spectra. The exposure time is automatically adapted to the amount of incident light so that the maximum signal in the individual spectra never exceed the point where the detector starts to saturate (se Figure 2.6). The total integration time is normally set to 300 s during which several individual spectra are recorded and co-added. Dark current spectra are measured once a day, normally when the SZA is below 96°. At Ny-Ålesund and Andøya, the SZA will never reach 96° for long periods. In these periods, the dark current spectra are measured during the day. The time is taken from a GPS (Global Position System) antenna which is connected to the PC. Measurements of atmospheric spectra are performed during the whole day whenever the SZA is higher than 96°. A block diagram of the program is in Figure 2.11.

Spectra are stored in one file per day in ascii format. Dark current spectra are saved in a separate file. The dark current is subtracted when analysing the spectra (see Chap. 2.3).

2.12 Instrumental Problems

Different instrumental problems have occurred during the period from autumn 1995 to 1999, and measurements could not always be performed. The first problem occurred already the first time the instrument was installed at Ny-Ålesund in August 1995. The temperature sensor at the detector head did not work properly, and the detector could not be cooled to sufficiently low temperatures (-40°C). This was probably due to damage during the transport from NILU to Ny-Ålesund. The detector and the detector controller were sent to Spectroscopy Instruments in Germany for repair. Measurement could therefore not start before 25 September.

The second time a problem with SYMOCS-VIS appeared was during the installation at ALOMAR[3] at Andøya in December 1997. The detector and the detector controller were sent to Germany for repair, but more or less the same problems were observed during the next installation. When the instrument was brought back to NILU it worked properly. This gave us an indication that the problem could be due to an electronic disturbance at ALOMAR (other groups had also experienced this). It was therefore decided that the instrument should be installed at Andøya Rocket Range (ARR). However, a new problem with the detector came up. The preamplifier board had been damaged. Finally, SYMOCS-VIS was installed at ARR 25 May 1998. During the installation at ARR it became clear that the detector was still not working properly. The entire detector had to be replaced, and the delivery time turned out to be more than 9 months. These series of problems resulted in total instrumental down time of more than one year. SYMOCS-VIS was finally re-installed at ARR on 25 March 1999. However, the detector broke down once again in July 1999. The fixed detector will be re-installed in February 2000.

[3] The Arctic Lidar Observatory for Middle Atmosphere Research

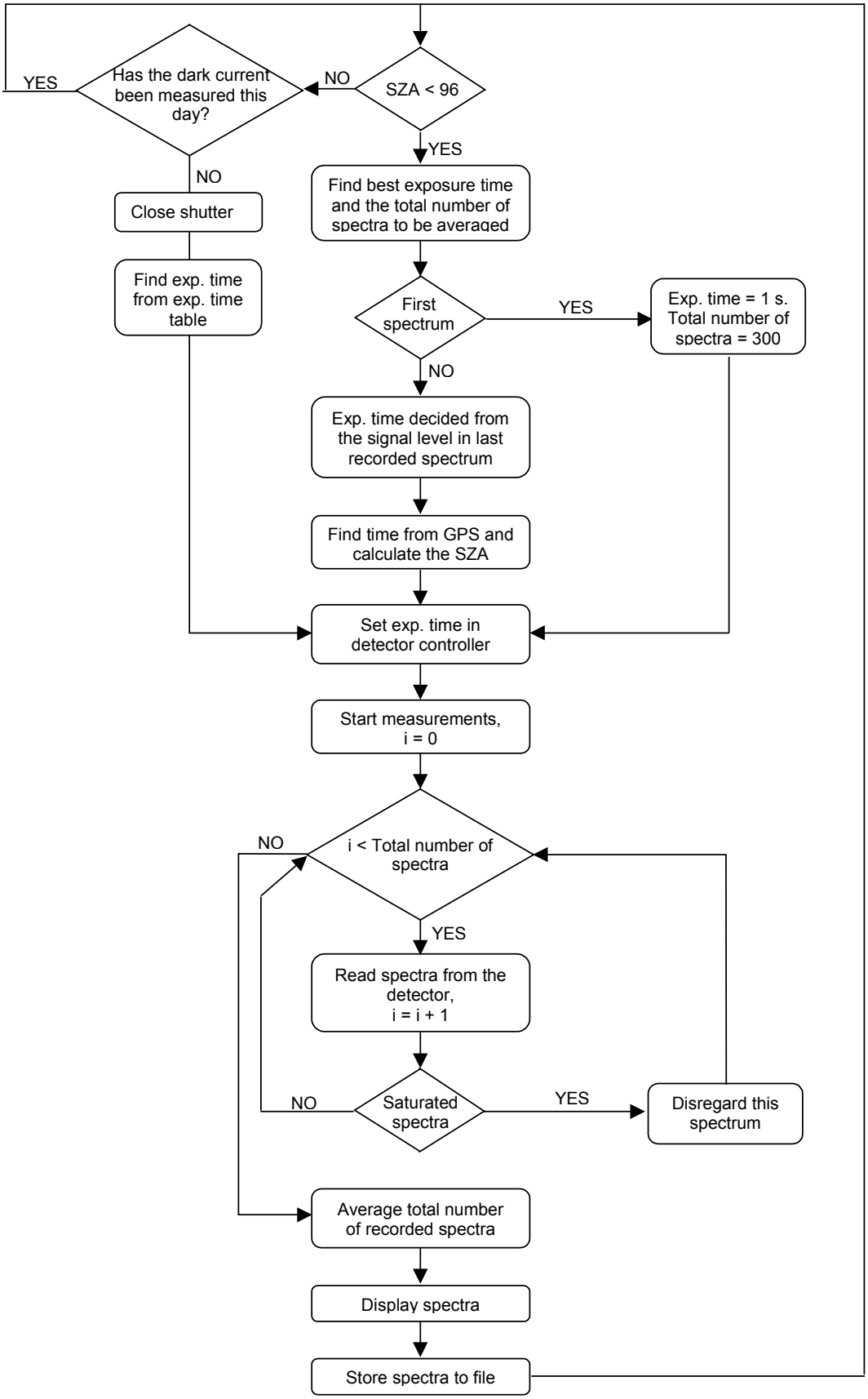

Figure 2.11: Block diagram of the SPEC-RUN software package used to control the measurements of the SYMOCS spectrometers.

3 UV-visible Spectroscopy

3.1 Viewing Geometry

There are two main measurement geometries used for spectroscopic UV-visible measurements of the atmosphere. In both geometries, the sun serves as the light source. One is direct absorption spectroscopy, in which the instrument views the light source directly. For the measurements presented in this report, the vertically pointing fibre collects scattered sunlight from the zenith and transmit the light into a spectrometer. The viewing geometry for a zenith sky measurement is shown in Figure 3.1. The received light has been scattered from a range of altitudes. The intensity of the scattered light is dependent on the density of the scatterers, which decrease exponentially with altitude. The intensity of light increases with height. This implies that one can define an altitude from which most of the scattered flux is coming. Above the scattering altitude the photons follow a slant path, τ_s, whereas below it they follow a vertical path, τ_v, as illustrated in Figure 3.2. The scattering altitude increases rapidly at increasing SZA and decreasing wavelengths. At 30° solar zenith angle and a wavelength of 440 nm, the scattering altitude is approximately 5 km, but at 90° the scattering altitude is approximately 15 km. At 93° the scattering altitude is around 25 km. At 350 nm the scattering altitude at 90° SZA is approximately 20 km.

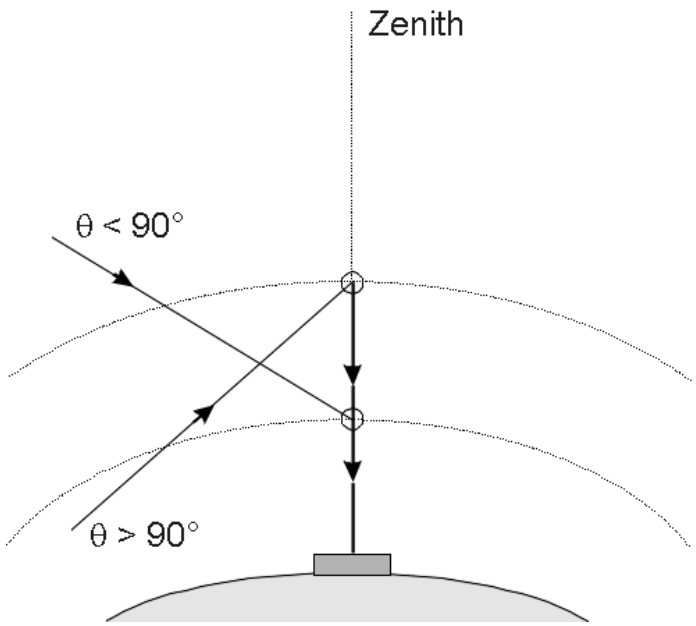

Figure 3.1: Ray geometry of the light seen by an instrument that measures the scattered light from the zenith sky.

The spectra are analysed by the method know as the Differential Optical Absorption Spectroscopy (DOAS). This method for measuring the absorption of visible and near-ultraviolet light scattered from the zenith sky is now well documented in the literature (e.g. Platt et al., 1979; Solomon et al., 1987). Observations of scattered light has several important advantages over observing direct light such as

- Measurements can be performed during twilight condition when the solar zenith angle is exceeds 90°,
- More sensitive to stratospheric absorbers due to the long light path through the stratosphere (especially at high solar zenith angles),
- Interference from tropospheric absorbers is minimal,
- Not limited to clear sky conditions, and
- Ease of automation, yielding good time resolution.

With a zenith viewing spectrometer, the quantity one measures is the slant column due to the slant path that the light has traversed. It is, however, of interest to convert the measured slant column to a vertical column of the absorber, because the vertical column shows the diurnal variation in the concentration more precisely. The slant column, $\tau_s+\tau_{v'}$, and the vertical column, τ_v, are illustrated in Figure 3.2.

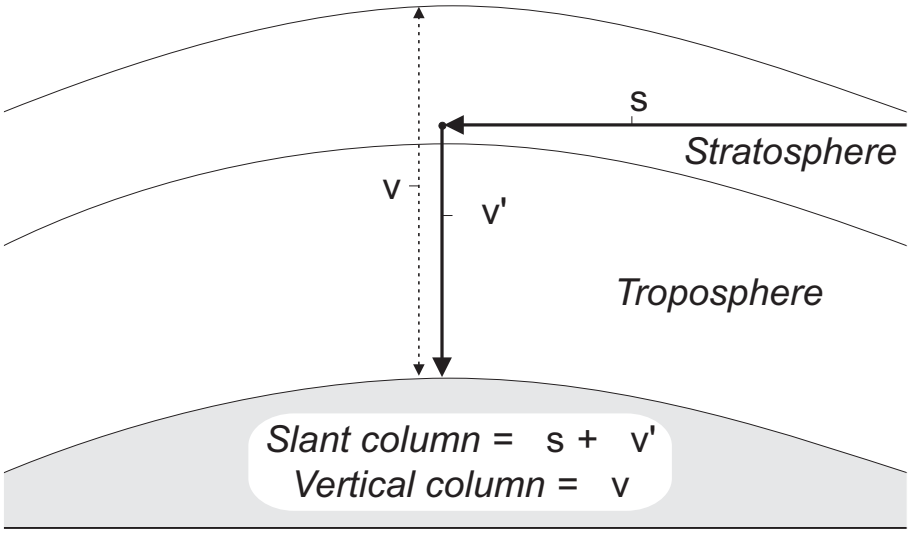

Figure 3.2: Illustration of the slant and the vertical column.

The output from the spectral analysis is the measured slant column of each compound fitted at one SZA minus the amount in a spectrum measured at a lower SZA. This value is called the differential slant column density (DSCD) and is described in the next section. The conversion of differential slant column to slant column, and conversion of the slant column to vertical column are described in more detail in Chap. 3.7.

3.2 The Principles of the DOAS Analysis Method

The fundamental principle underlying absorption measurements is the Beer-Lambert law

$$I(\lambda) = I_0(\lambda)\exp\{-n\sigma_a(\lambda,T)\}, \qquad \textit{Eq. 3.1}$$

where $I_0(\lambda)$ is the incident intensity to the absorbing media, and $I(\lambda)$ is the transmitted intensity through the absorbing media. $\sigma_a(\lambda,T)$ is the wavelength and

temperature dependent absorption cross section of the absorbing molecules and *n* is the number of absorbing molecules per unit area. *n* is the slant column amount of the absorber (slant column because the light has traversed a slant path). The product $[n\sigma_a(\lambda,T]$ is called the optical depth, $\tau(\lambda)$. If there are several absorbing molecules, the Beer-Lambert law becomes

$$I(\lambda) = I_0(\lambda)\exp\left\{-\sum_i\left(\sigma_i(\lambda,T)n_i\right)-\varepsilon_{Ray}(\lambda)-\varepsilon_{Mie}(\lambda)\right\}. \qquad \textit{Eq. 3.2}$$

Here, scattering by air molecules (Rayleigh scattering) and by aerosols (Mie scattering) is included. $\varepsilon_{Ray}(\lambda)$ is the Rayleigh scattering coefficient, and $\varepsilon_{Mie}(\lambda)$ is the Mie scattering coefficient.

For zenith sky measurements, $I_0(\lambda)$ is the extraterrestrial solar spectrum (irradiance). By dividing two spectra measured by the instrument where the light has traversed different atmospheric paths, $I_0(\lambda)$ together with the instrumental wavelength response are eliminated. The atmospheric absorption, which differ between the two spectra due to the change in the light path or observed airmass, remains.

$$\frac{I_1(\lambda)}{I_2(\lambda)} = \frac{I_0(\lambda)\exp\left\{-\sum_i\left(\sigma_i(\lambda,T)n_{i,1}\right)-\varepsilon_{Ray,1}(\lambda)-\varepsilon_{Mie,1}(\lambda)\right\}}{I_0(\lambda)\exp\left\{-\sum_i\left(\sigma_i(\lambda,T)n_{i,2}\right)-\varepsilon_{Ray,2}(\lambda)-\varepsilon_{Mie,2}(\lambda)\right\}} \qquad \textit{Eq. 3.3}$$

For zenith sky measurements, the $I_1(\lambda)$ is normally a spectrum taken at low sun, and the $I_2(\lambda)$ is taken at high sun and therefore contains little absorption.

The difference in optical depth, $\Delta\tau(\lambda)$, between two zenith sky spectra may then be calculated by taking the logarithm of the ratio of the spectra.

$$\Delta\tau(\lambda) = -\ln\left(\frac{I_1(\lambda)}{I_2(\lambda)}\right) = \sum_i\left(\sigma_i(\lambda,T)\left(n_{i,1}-n_{i,2}\right)+\Delta\varepsilon_{Ray}(\lambda)+\Delta\varepsilon_{Mie}(\lambda)\right), \qquad \textit{Eq. 3.4}$$

where $\Delta\varepsilon_{Ray}(\lambda) = \varepsilon_{Ray,1}(\lambda) - \varepsilon_{Ray,2}(\lambda)$ and $\Delta\varepsilon_{Mie}(\lambda) = \varepsilon_{Mie,1}(\lambda) - \varepsilon_{Mie,2}(\lambda)$. The absorption structures due to Rayleigh and Mie scattering are broad band features, whereas the absorption due to molecules are narrow band features. The broad band features can be removed by either filtering techniques or by fitting a low order polynomial. The logarithm of the ratio of the two spectra are then divided by the low order polynomial to remove the broad band structure. The software used in this work provides polynomial fitting. The optimal degree of polynomial to use is dependent on the width of the wavelength region. It is important to keep the numbers of fitted parameters to a minimum to reduce the amount of unknown variables. After removing the structures due to Rayleigh and Mie scattering, Eq. 3.4 is simplified to

$$\Delta\tau(\lambda) = -\ln\left(\frac{I_1(\lambda)}{I_2(\lambda)}\right) = \sum_i\left(\sigma_i(\lambda,T)\left(n_{i,1}-n_{i,2}\right)\right). \qquad \textit{Eq. 3.5}$$

Providing the absorption cross sections of the absorbing molecules are sufficiently dissimilar, the differential slant columns of all absorbers can be determined simultaneously by a least-square fit of the absorption cross sections to the ratio spectrum. The magnitude of the difference between the observed and fitted optical depths (the residual) is a measure of the quality of the fit. The spectral residuals may display common features. These structures could be caused by unknown absorbers in the atmosphere or instrument artefacts, but also by systematic errors in the treatment of the included parameters, such as the gas temperature used when measuring the molecular cross sections. As mentioned earlier, the cross sections can be strongly temperature dependent. It is therefore important to use cross sections measured in the laboratory at temperatures that are typical for the stratospheric in order to: (i) to retrieve the 'true' value of the compound and (ii) to increase the ability to measure weaker absorbers by reducing the remaining residual features between the measured spectrum and the laboratory cross sections. In Figure 3.3, the spectra after the different steps in the procedure of the DOAS analysis method are plotted to illustrate the method.

Before the ratio of the two spectra is calculated, the spectra have to be carefully wavelength aligned. This is required even though the two spectra are measured with the same instrument. Due to slight variations in the instrument temperature, the spectral image on the detector can become displaced. This effect is accounted for in the analysis software.

3.2.1 WinDOAS

The analysis software used at NILU has been developed at BIRA-IASB[4] by Michel Van Roozendael and Caroline Fayt, and is called WinDOAS. It includes a coupled linear/non-linear least-squares algorithm (SVD/Marquard-Levenberg). The software is written in C++ and the interface is very user-friendly and runs under Windows 95/98 and NT. The software package includes many advanced DOAS-features such as I_0 correction, wavelength calibration using high resolution Fraunhofer spectra, convolution of reference cross sections to the instrument resolution and calculation of theoretical Ring cross section. These DOAS-features will be described in more detail in the following sections.

[4] Belgian Institute for Space Aeronomy, Brussels, Belgium

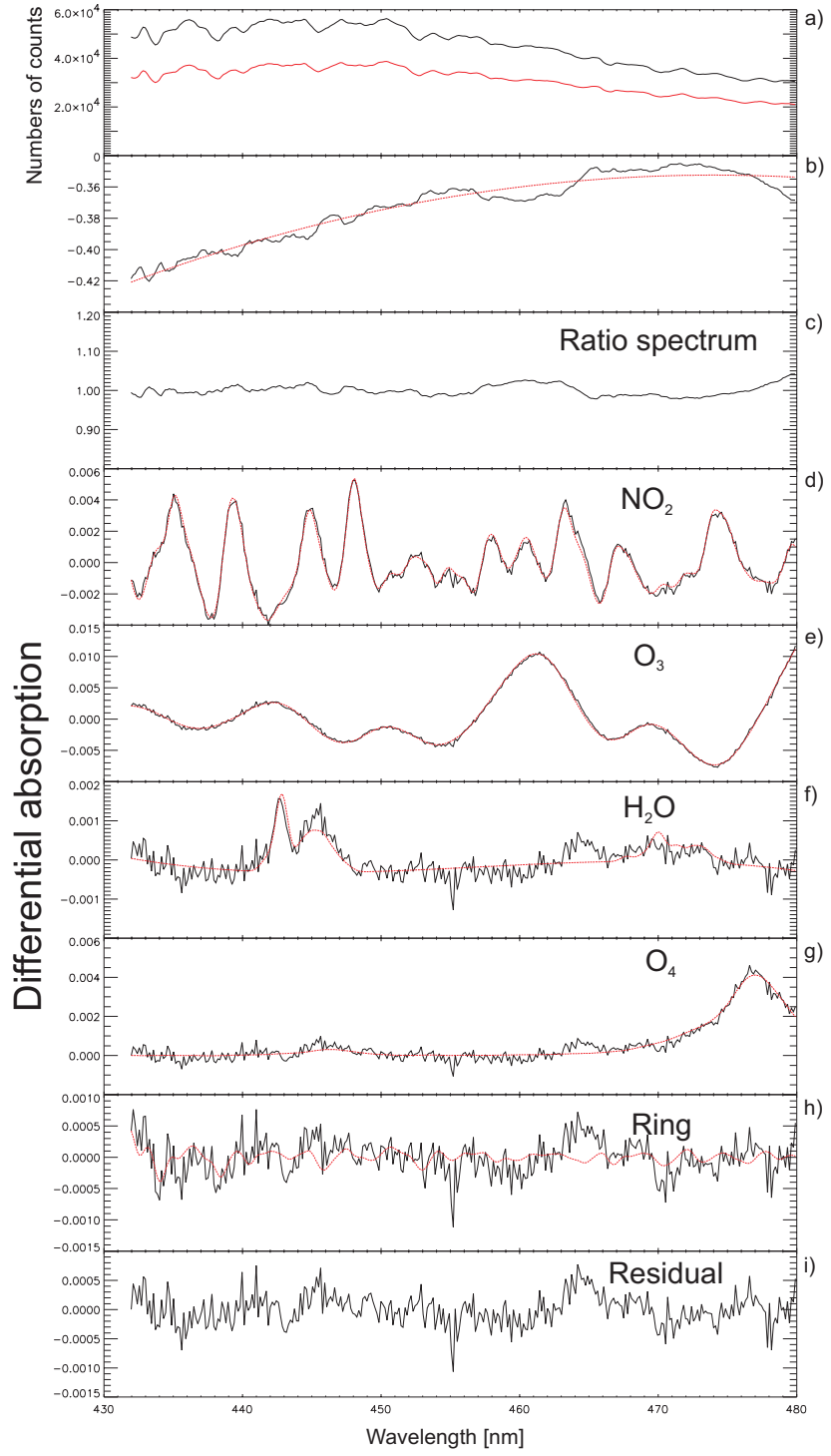

Figure 3.3: In a) a spectrum at high sun in black (reference spectrum taken at 26 March at 76.5° SZA) and at low sun in red taken at 90.1° SZA on 23 March 1996 is shown for the wavelength region 430-480 nm. In b) the logarithm of the ratio between the two spectra is shown together with the fitted third degree polynomial. The result after removal of broad band features is seen in (c). In (d)-(h) the absorption cross section to the different absorbers (red line) are shown together with the measured differential spectrum (solid black line). Panel (i) shows the residual spectrum.

3.3 Cross Sections

The quality of the retrieval of the differential slant columns of the various stratospheric compounds is highly dependent on the quality of the reference absorption cross section used in the fitting procedure. The precision of the wavelength calibration as well as the accuracy of the absolute absorption cross section values are very important for a correct retrieval of the slant or vertical columns. The quality of the reference absorption cross sections available for zenith sky measurements has improved in recent years. Most important is that the newest measured cross sections are measured by Fourier Transform Spectrometers providing high resolution cross sections with a very accurate wavelength calibration. The absorption cross sections used in this work are all measured by instruments other than SYMOCS-VIS or SYMOCS-UV. These cross sections must therefore be convoluted with the ILS function of our instrument to match the resolution of our instruments. The convolution procedure is based on the following equation

$$XS_f(\lambda') = \frac{\int XS(\lambda'-\lambda)F(\lambda)d\lambda}{\int F(\lambda)d\lambda}, \qquad \textit{Eq. 3.6}$$

where $XS_f(\lambda')$ is the convoluted cross section, $XS(\lambda)$ is the reference cross section and $F(\lambda)$ is the ILS function. A procedure for doing this is included in the analysis software provided by BIRA-IASB.

For a meaningful convolution process, it is important that the spectral resolution of the reference cross section is sufficiently high compared to the spectral resolution of the field instrument. The molecular absorption cross sections presently in use in the DOAS analysis of the SYMOCS spectra are listed in Table 3.1, and shown in Figure 3.4.

Table 3.1: Listing of the molecular reference cross sections used in this work.

Cross section	***Temperature***	***Resolution***	***Instrument***	***Reference***
O_3	221 K 241 K	Wavelength dependent, 0.2-0.3 nm	GOME FM satellite Spectrometer (grating spectrometer)	Burrows et al., 1999
NO_2	227 K	0.03 nm	Fourier Transform Spectrometer	Harder et al., 1997
O_4	298 K	0.03 nm	Fourier Transform Spectrometer	Hermans et al., 1999
H_2O	298 K		HITRAN-96	Rothman et al., 1998
BrO	228 K	0.4 nm	Grating spectrometer	Wahner et al., 1988
OClO	213 K	~0.01 nm	Fourier Transform Spectrometer	Kromminga et al., 1999

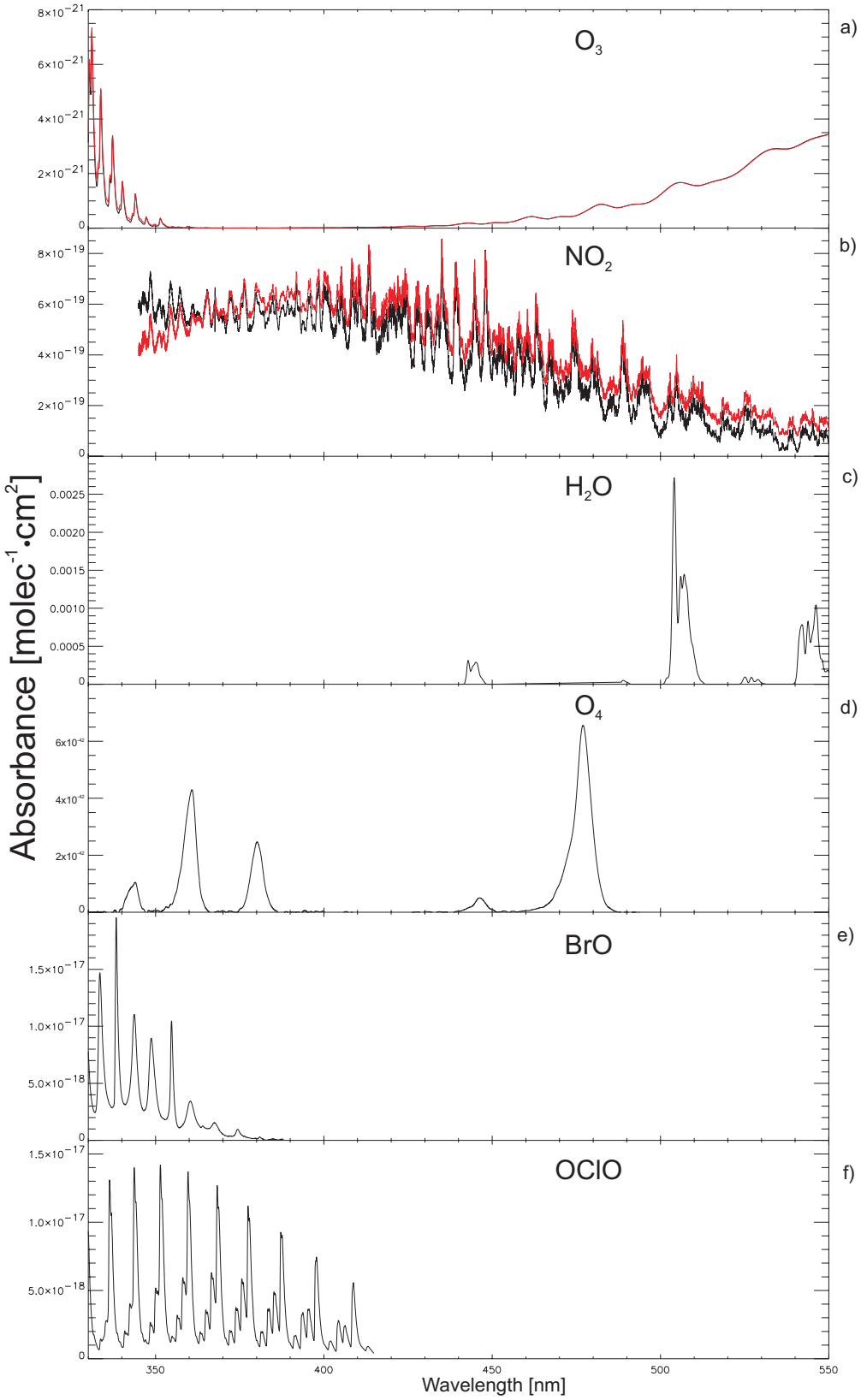

Figure 3.4: The molecular reference cross sections listed in Table 3.1 plotted from 330-550 nm. (a) Ozone at two different temperatures (221 K in black and 241 K in red), (b) NO_2 at two different temperatures (227 K in black and 294 K in red), (c) H_2O (298 K), (d) O_4 (298 K), (e) BrO (228 K) and (f) OClO (213 K).

3.3.1 O_3

The absorption cross section of O_3 is strongly temperature dependent in the Huggins band (310-350 nm), but not in the Chappius band (430-550 nm). In this work, the low temperature O_3 cross section measured by the FM GOME Spectrometer (Burrows et al., 1999) was used. FTS studies of high resolution O_3 cross sections carried out by the University of Bremen (Voigt et al., 2000) have indicated that the GOME-O_3 cross sections are calibrated approximately 0.03 nm too low in wavelength. FTS high-resolution cross sections have an accurate wavelength calibration and tend to be more reliable. However, they need to be further tested before implemented in the analysis.

Since the O_3 cross section shows a strong temperature dependence in the UV and is the dominating absorber (especially in the BrO analysis window), two different cross sections measured at two different temperatures are fitted simultaneously in order to approximately account for the effect of having O_3 at different temperatures in the stratosphere. The method of fitting two or more cross sections of the same molecule was first proposed by Sanders (1996). Sanders showed the effect for the analysis of NO_2 in the visible region.

3.3.2 NO_2

In the 400-480 nm region of the atmospheric spectrum, NO_2 absorptions are larger than 1%. NO_2 is therefore detected in this part of the spectrum. However, to be able to measure weaker absorbers such as OClO and IO, it is important to remove the absorption features of NO_2 completely. The temperature dependency of the NO_2 absorption cross section is low in the UV part of the spectrum, but increases towards longer wavelengths. The NO_2 differential slant columns retrieved in the 430-480 nm wavelength region, decrease by approximately 20% when applying a low temperature NO_2 cross section instead of one measured at room temperature. Results show that the residuals are reduced when using a cross section measured at a temperature that is representative of the stratosphere. The high resolution NO_2 cross section measured at 227 K by Harder et al. (1997) has been used in the standard analysis. This cross section has a very accurate wavelength calibration.

3.3.3 O_4

O_4, the dimer of O_2, is commonly in stratiform clouds. On cloudy days the absorption due to O_4 can be significant. Recent high resolution FTS measurements of the O_4 cross section performed both in the UV and the visible are implemented in the standard analysis (Hermans et al., 1999). The measurements are performed at atmospheric pressure in contrast to the commonly used O_4 cross section of Greenblatt et al. (1990) which were made at a pressure of 600 atm.

3.3.4 H_2O

The H_2O absorption cross section is taken from the HITRAN database (Rothman et al., 1998).

3.3.5 BrO

The cross section of Wahner et al. (1988) measured at 228 K has been used in this study with the necessary shift. Aliwell et al. (1997) found that this cross section

has to be wavelength shifted +0.17 nm to match the BrO features in the measured spectra. The resolution of the Wahner et al. (1988) cross section is only about 0.4 nm. High-resolution cross sections of BrO have been measured by using a FTS at the University of Bremen for different temperatures. They will soon be available to the scientific community (O. Fleischmann, http://www-iup.physik.uni-bremen.de/gruppen/Data.html, 20 December 1999).

3.3.6 OClO

Until recently the cross section of Wahner et al. (1987) measured at 204 K was used in the standard analysis. The wavelength calibration of this cross section is also poor, and the wavelength shift is dependent on the wavelength region. For the 357-385 nm wavelength region (the OClO window), a shift of approximately +0.177 nm is found to be necessary. In 1999 a new cross section of OClO measured by the University of Bremen became available to the scientific community (Kromminga et al., 1999). This high resolution cross section was measured by FTS, and the wavelength accuracy is expected to be good. Using this cross section compared to the Wahner cross section, the differential slant columns of OClO increased by approximately 15%. However, the residual was not significantly improved.

3.3.7 The Solar I_o effect

The need to correct the cross sections for the solar I_0-effect arises from the difference in cross sections measured in the laboratory with a smooth light source and those 'seen' by the atmosphere with a structured solar light source (Johnston, 1996). The cause of the problem is that a complete removal of the Fraunhofer spectrum by forming the log ratio of a twilight to a midday spectrum is not possible. The reason is that the measured spectra in the DOAS-ratio (see Eq. 3.3) have been filtered by the instrument line shape function before the ratio is calculated. The filtered spectra measured at high sun, $I_{midday,f}(\lambda)$, and at twilight, $I_{twilight,f}(\lambda)$, can be written as (convolution of the Lambert–Beers law):

$$I_{midday,f}(\lambda') = \frac{\int I_0(\lambda'-\lambda)F(\lambda)d\lambda}{\int F(\lambda)d\lambda}, \qquad \textit{Eq. 3.7}$$

$$I_{twilight,f}(\lambda') = \frac{\int I_0(\lambda'-\lambda)e^{-h(\lambda)}F(\lambda)d\lambda}{\int F(\lambda)d\lambda}, \qquad \textit{Eq. 3.8}$$

where $F(\lambda)$ is the ILS function and $e^{-h(\lambda)}$ is the optical depth of an absorber. The I_0-term will not be completely removed when calculating the log-ratio of the two spectra unless either $I_0(\lambda'-\lambda)$ or the $h(\lambda)$-term are constant over the integration interval. The integration interval is from the negative to the positive edge of the ILS). The corrections to the cross sections are made according to the following equation (Johnston, 1996)

$$\sigma_{I_0-corr}(\lambda) = -\ln\left(\frac{\sigma(\lambda)}{sol(\lambda)}\right) * \frac{1}{x}, \qquad \textit{Eq. 3.9}$$

where x is a chosen amount of absorber column (typically the maximum measured), $\sigma_{Io\text{-}corr}(\lambda)$ is the I_0-corrected cross section, $\sigma(\lambda)$ is the laboratory measured absorption cross section and $sol(\lambda)$ is the high resolution solar Fraunhofer spectrum. The effect on the ozone cross section when correcting for the I_0-effect is illustrated in Figure 3.5.

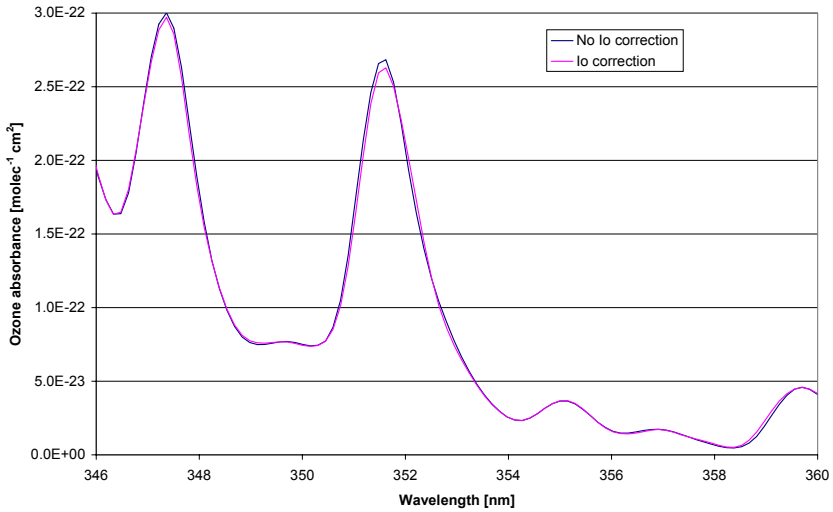

Figure 3.5: Effect on the ozone cross section in the 346 to 360 nm wavelength region when applying the I_0-effect in the convolution process.

This correction is usually applied for cross sections that vary significantly as a function of wavelength such as O_3, NO_2, BrO and OClO in the UV-region, and for NO_2 and OClO in the visible region. Analysing synthetic atmospheric spectra is a powerful tool for studying the effects of e.g. using I_0 corrected cross sections compared to non-I_0 corrected cross sections without the limitations of spectral quality. Through the work, which is summarised in Aliwell et al. (2000), synthetic spectra produced by NIWA[5] with known amounts of various absorbers (O_3, NO_2, BrO, Ring), were analysed with and without I_0 corrected O_3 cross sections. As described in Chapter 3.3.5, two ozone cross sections at different temperatures (221 K and 241 K) are used in the retrieval of BrO. When using uncorrected cross sections, the relative concentrations fitted by two different ozone cross sections are incorrect, but the sum of fitted ozone approximately equals the sum of the generated ozone in the synthetic spectrum. The retrieved BrO differential slant column is too high compared to the generated BrO amount. This is most probably due to misalignment of the O_3 absorption features as a result of not including a correction for the solar I_0-effect. The analyses process tries to compensate for the less than optimum alignment by fitting more 241 K O_3 and less 221 K O_3. Due to inadequacies of the compensation and a correlation of remaining features with BrO cross section, the fitted BrO amount is too high. However, when applying the I_0 correction on the O_3 cross sections, the fitted O_3 (221 K), O_3 (241 K) and the BrO differential slant column equal the generated amounts, indicating that a correction of the solar I_0-effect is essential for the retrieval of BrO. These results are given in Table 3.2.

[5] National Institute of Water and Atmospheric Research, Otaga, New Zealand

Table 3.2: Effects on the slant column of O_3, NO_2 and BrO retrieved from synthetic atmospheric spectra using non-I_0 and I_0 corrected O_3 cross sections. The actual amounts in molec/cm^2 are given in the first row.

Analysing method	O_3 (221 K)	O_3 (241 K)	NO_2	BrO
Actual amount	8.00	2.00	5.00	1.50
Non-I_0 corrected O_3 cross section	6.50	3.49	4.93	2.00
I_0 corrected O_3 cross section	8.03	1.97	5.00	1.50

The I_0 correction also improves the quality of the fit in the analysis procedure and has been applied to O_3 and NO_2 in the UV-region for the analysis of BrO and OClO, as illustrated in Figure 3.6 and Figure 3.7. In fact, using I_0 correction was one of the recommendations from the comparison workshop on the retrieval of BrO at OHP in 1996 (Aliwell et al., 2000). Figure 3.8 shows the effect on the BrO columns when not using I_0 corrected O_3 and NO_2 cross sections when analysing atmospheric spectra. In Figure 3.8, BrO columns retrieved from SYMOCS spectra from PM 26 June 1996 (OHP) is shown. On this particular day, the use of I_0 corrected O_3 cross sections is seen to decrease the BrO differential slant column by 24% at 90° SZA. The BrO slant column decreased even more (29%) by applying a I_0 corrected NO_2 cross section as well. Using I_0 corrected BrO cross sections had no effect on the BrO differential slant column. It is most essential to correct the O_3 (and NO_2) cross sections for the solar I_0-effect since these compounds are the strongest absorbers in the wavelength region.

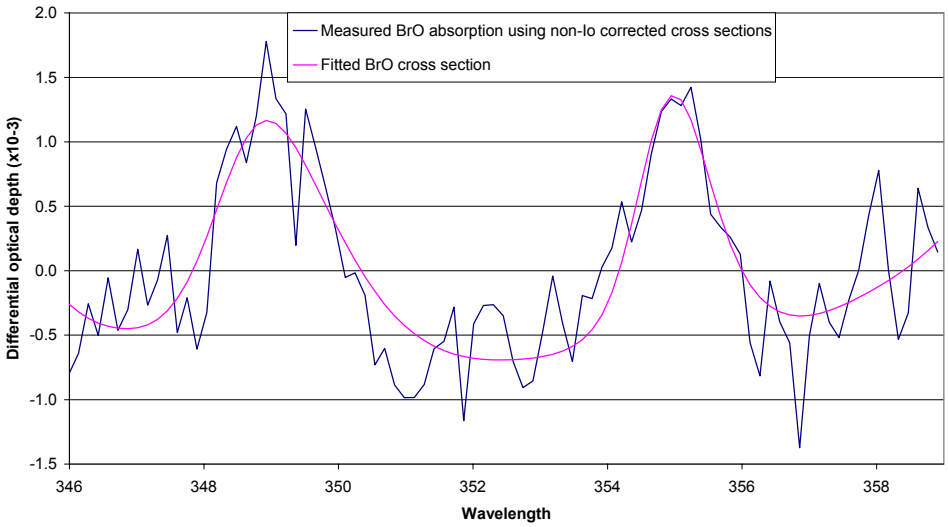

Figure 3.6: An example of the fitting of BrO when using non-I_0 corrected cross sections. The spectrum is from 26 June 1996 at OHP (SZA=90°, PM).

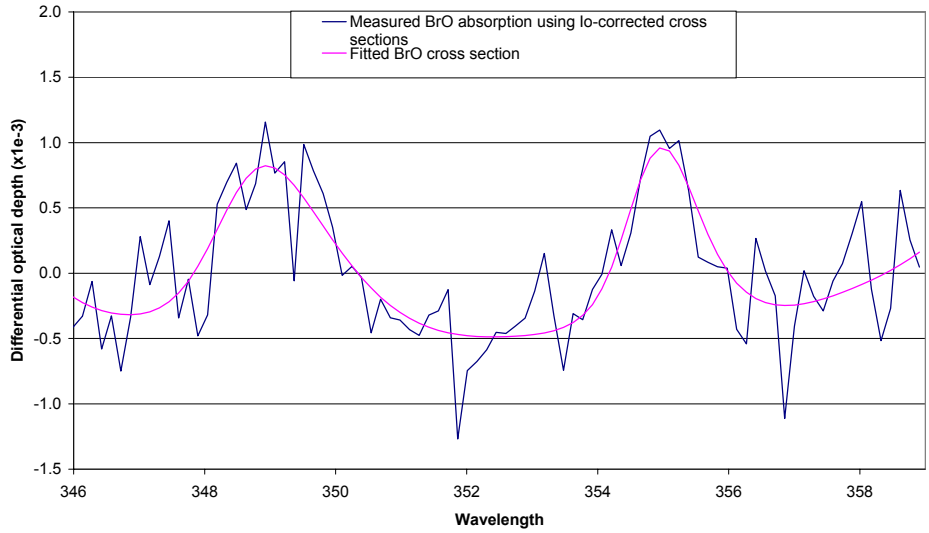

Figure 3.7: An example of the fitting of BrO when using I_0 corrected cross sections. The spectrum is from 26 June 1996 at OHP (SZA=90°, PM).

I_0 correction of NO_2 cross sections has no effect on the NO_2 amount (nor the residual) when retrieving NO_2 differential slant columns in the visible region, for both high and low NO_2 concentrations. It is important to note that this test has only been applied on real atmospheric spectra. However, the effect is also non-significant for synthetic spectra for the 430-480 nm wavelength region (Johnston, personal communication). Still, I_0 corrected NO_2 cross sections have been used in the analysis of NO_2 in the visible region.

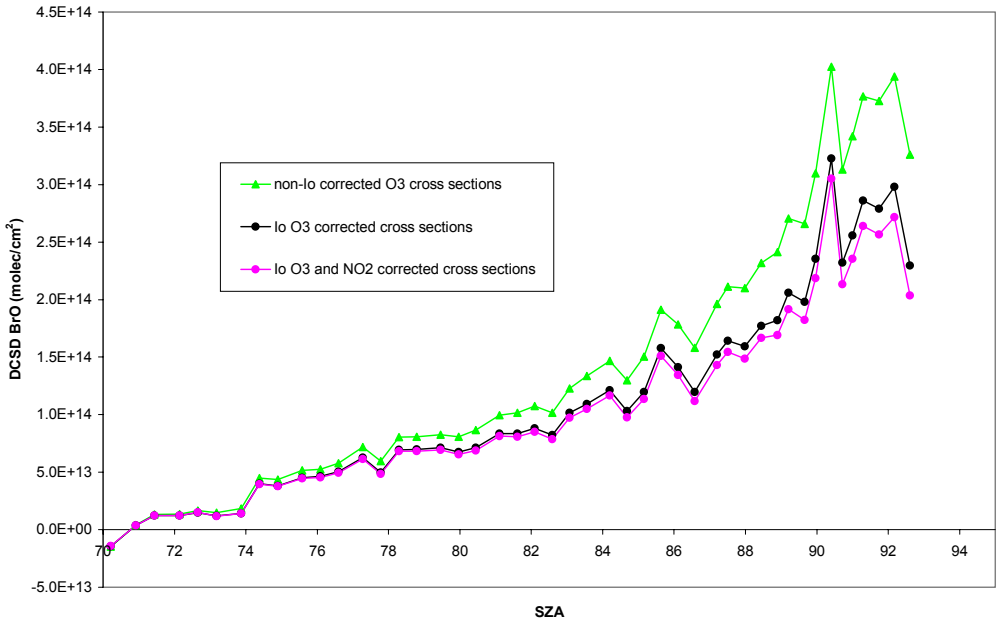

Figure 3.8: An example of a comparison of differential slant column densities of BrO on 26 June 1996 (PM) at OHP using (i) I_0 corrected O_3 and NO_2 cross sections (pink circles), (ii) I_0 corrected O_3 cross sections (black circles) and (iii) non-I_0 corrected O_3 and NO_2 cross sections (green triangles).

3.4 Treatment of Offsets in the Spectra

An offset in the spectra due to e.g. stray light or improper subtraction of the dark current can be accounted for in the analysis. A constant offset in an observed spectrum may be corrected for by fitting the inverse of the spectrum itself in the same way as the molecular cross section spectra. This is seen from the following equations

$$I(\lambda) = I_0(\lambda)\exp(-\tau) + C, \qquad \textit{Eq. 3.10}$$

where $I_0(\lambda)$ is the extraterrestial solar spectrum, τ is the cumulative optical depth of the atmospheric absorbers and C is a constant offset. In the DOAS-method, two spectra measured at different SZA are divided,

$$-\ln\left(\frac{I_1(\lambda)}{I_2(\lambda)}\right) = -\ln\left(I_0(\lambda)\exp(-\tau_1) + C_1\right) + \ln\left(I_0(\lambda)\exp(-\tau_2) + C_2\right). \qquad \textit{Eq. 3.11}$$

If the optical depths are sufficiently small, the approximations $\exp(-x) \approx 1-x$ and $\ln(1+x) \approx x$ can be applied, and hence

$$-\ln\left(\frac{I_1(\lambda)}{I_2(\lambda)}\right) = \tau_1 - \tau_2 + \frac{C_2 - C_1}{I_0(\lambda)}. \qquad \textit{Eq. 3.12}$$

Both stray light and the dark current offset can have structures. Then a slope of second order can be fitted (Van Roozendael, personal communication). There are good reasons to include offset fitting in the spectral analysis, since almost all spectrometers have some straylight. The use of an offset fit depends on the measurements in order to improve fits and residuals. Experience shows that especially the BrO results can be affected by the choice of constant or slope offset fit. It is not obvious which type of offset fitting that will be the most "correct". In Figure 3.9, retrieved differential slant columns of BrO from 26 June 1996 at OHP (SYMOCS) and 3 March 1999 at Andøya (SYMOCS-UV) are shown for (i) no offset fitted, (ii) constant offset and (iii) offset fitted like a slope. The BrO values at high SZA are most affected. It is interesting to note that the results are almost the same for the second instrument measured at another site and season The results from the sensitivity test are summarised in Table 3.3.

Table 3.3: Effect on the retrieved BrO differential slant columns at 90° SZA when applying no offset correction, a constant offset correction or a offset correction like a slope.

		(Const offset-No offset)/No offset	(Slope offset-No offset)/No offset
SYMOCS (26 June 1996)	AM PM	6% 13%	11% 17%
SYMOCS-UV (2 March 1999)	AM PM	9% 15%	9% 13%

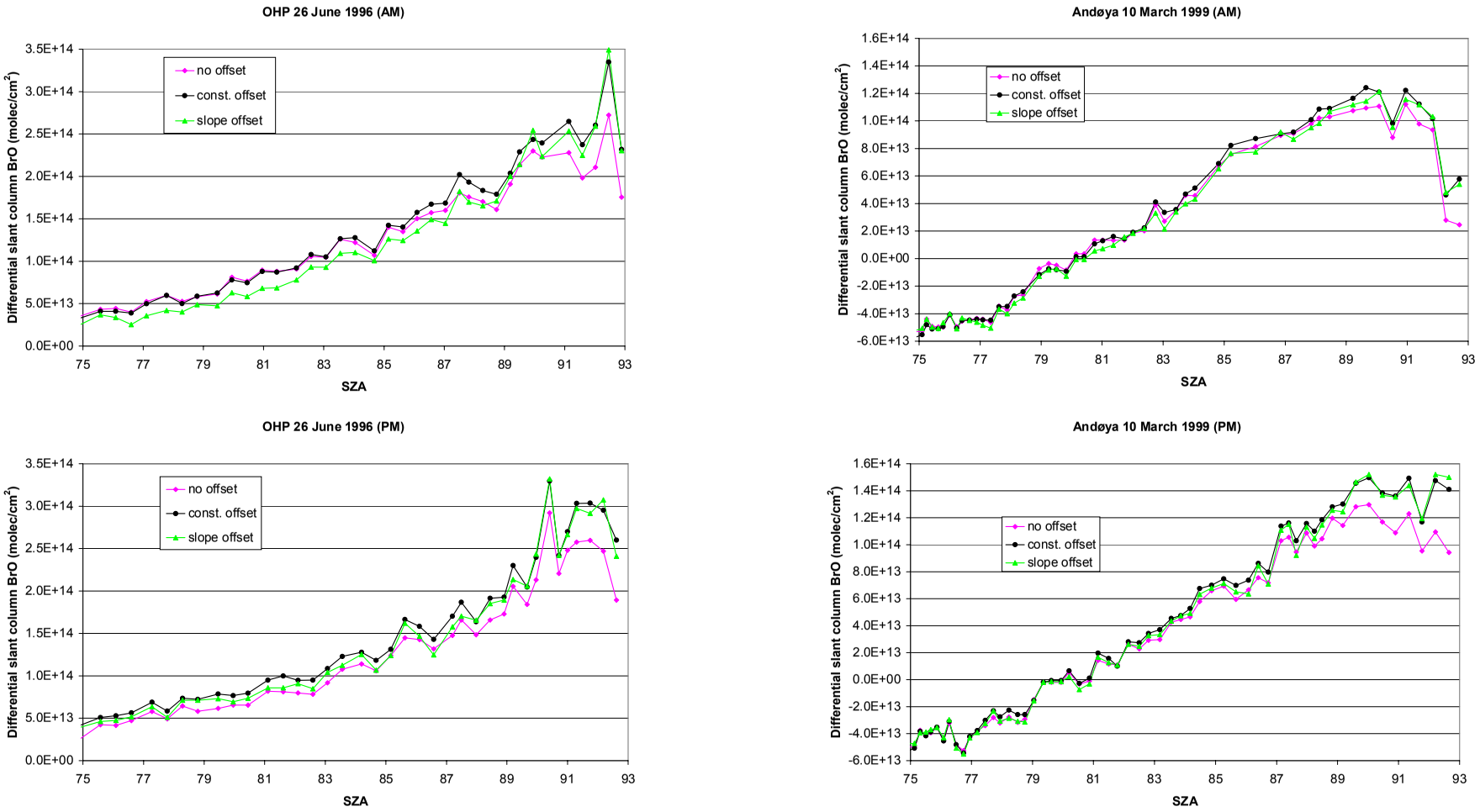

Figure 3.9: Effect on BrO amounts when using no offset fitting (pink circles) in the analysis compared to constant (black circles) or slope fitting (green triangles). In the two left panels, measurements performed by SYMOCS (26 June 1996 at OHP) are shown. In the two right panels, measurements from SYMOCS-UV the 3 March 1999 are plotted.

The effect of using various offset fits on differential slant columns of OClO is also significant. OClO differential slant columns from 20 March 1997 (Ny-Ålesund) retrieved by using no offset, constant offset and offset fitted like a slope are plotted in Figure 3.10. The difference varied for one day to another, but common for all days tested is that the residual was lowest when fitting the offset as a slope. At 89.9° SZA, the AM OClO value decreased with 10% when fitting the offset as a slope compared to no offset fitted, whereas the value increased with 9% when using constant offset compared to no offset. The corresponding values for PM (89.9° SZA) are 3% decrease and 4% increase.

In the standard analysis used in this work, an offset like a slope is fitted in the BrO and OClO analysis. For the retrieval of NO_2 and O_3 a constant offset is fitted to account for possible stray light in the measurements even though the difference in differential slant columns when fitting an offset compared to not is less than 2% for NO_2 and less than 0.5% for O_3.

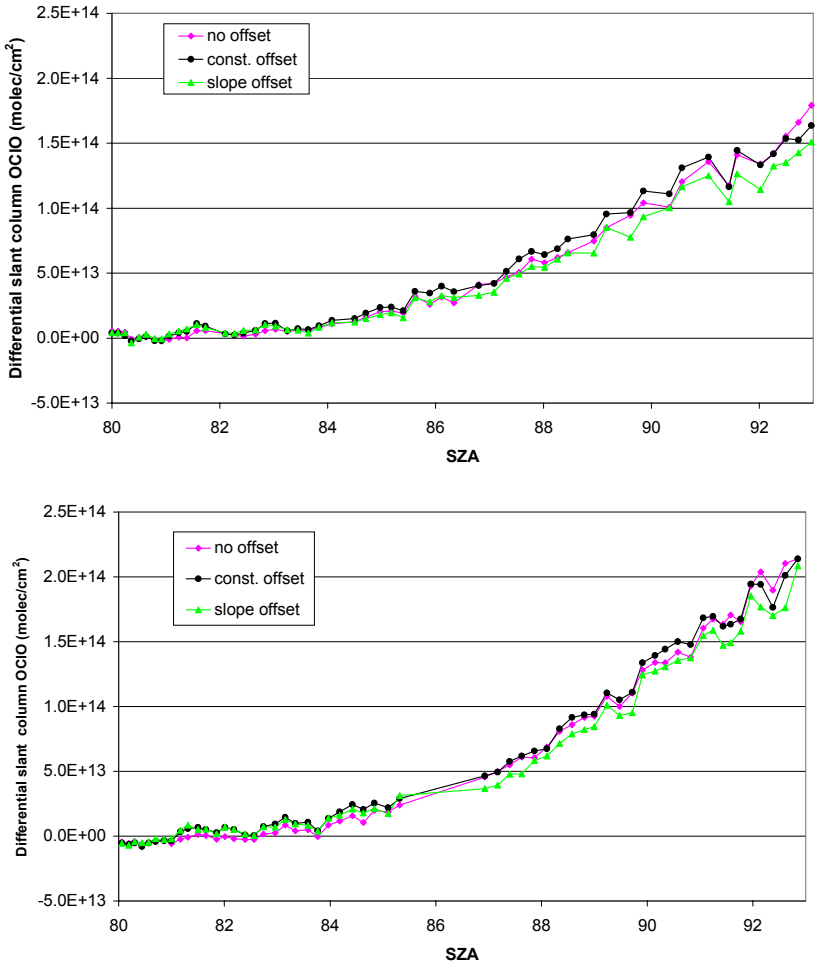

Figure 3.10: Effect on OClO amounts when using no offset fitting (pink circles) in the analysis compared to constant (black circles) or slope fitting (green triangles). Here data from 20 March 1997 (Ny-Ålesund) are shown.

3.5 The Ring Effect in Zenith Sky Spectra

When scattered sunlight is observed, the optical depths of the solar Fraunhofer lines are reduced relative to the Fraunhofer lines in direct sunlight (Grainger and Ring, 1962). This phenomenon is known as the Ring effect. Modelling of the Raman scattering cross section supports the theory that rotational Raman scattering is the major cause of the Ring effect (Fish et al., 1995). This effect is treated as all other absorbers and scatteres, that is in a Beer-Lambert's law formalism (Solomon et al., 1987). Rotational Raman scattering also reduces the optical depths of molecular absorptions resulting in an underestimation of the slant columns by 8% for NO_2 at 90° SZA (Fish et al., 1995). For the more broad-banded O_3 absorption structure, the effect is less than 1%. Since both BrO and OClO are narrow-banded like NO_2, the effect is expected to be of the same order as for NO_2. It is shown that the spectral structure of the Ring effect is relatively independent of location, season and solar zenith angle (Richter, personal communication). However, the fractional Ring intensity of the incoming light is constant (~ 6%) during full daytime, but increases sharply during twilight (Conde et al., 1992), which can be explained by increased multiple scattering at high SZA. Consequently, when two zenith sky spectra are ratioed (see eq. 3.3) in order to eliminate features in I_0, the Ring effect introduces structures into the ratio at wavelengths corresponding to the locations of the Fraunhofer lines. The magnitude of these residual features is comparable to the magnitude of absorptions due to BrO and NO_2. These residual features can therefore interfere or mask the absorption features of the absorbers.

During this work, both measured and calculated Ring cross sections have been used in the analysis. The measurements are performed as described in Solomon et al. (1987) by using a polariser. The difference in the degree of polarisation of Raman and Rayleigh scattered light are used to estimate an effective Ring cross section. The Rayleigh scattered light from the zenith sky is strongly polarised, and the Rayleigh scattering cross section can be separated into its parallel ($\sigma_{Ray||}$)and perpendicular ($\sigma_{Ray\perp}$) component [6], (Penndorf, 1957)

$$\begin{aligned}\sigma_{Ray\perp} &= 0.7629\sigma_{Ray} \\ \sigma_{RayII} &= 0.7629(0.9324\cos\varphi)2\sigma_{Ray}\end{aligned} \qquad \textit{Eq. 3.13}$$

φ is the angle between incoming and scattered rays.

Rotational Raman scattered light is unpolarised. This means that one can derive the desired Raman cross section, σ_{Ram}, from the ratio, R, of the intensities measured with parallel and perpendicular polarisation

$$R = \frac{I_{II}}{I\perp} = \frac{\sigma_{RayII} + \sigma_{Ram}}{\sigma_{Ray\perp} + \sigma_{Ram}}. \qquad \textit{Eq. 3.14}$$

[6] Note the incorrect labelling in Solomon et al. 1987

Rearranging this yields an expression for σ_{Ram}

$$\sigma_{Ram} = \frac{R\sigma_{Ray\perp} - \sigma_{RayII}}{1 - R}. \qquad \textit{Eq. 3.15}$$

It is common practice to define the Ring cross section as the Raman cross section relative to the Rayleigh cross section which gives (assuming φ=90°)

$$\sigma_{Ring} = \frac{R}{1 - R}. \qquad \textit{Eq. 3.16}$$

To be able to measure the Ring cross section, one needs a clear blue sky. This does not always coincide with the time of installation of the field instrument. The retrieval of the different atmospheric compounds from zenith sky spectra using either a theoretical Ring cross section or a measured Ring cross section of good quality, give similar results. However, a synthetic Ring cross section is very useful when there are frequent changes to the instrument resolution function or wavelength region covered. This has been the case for SYMOCS since the instrument has been moved several times since the first installation in 1995. It was therefore decided to use synthetic Ring cross section instead of measured Ring cross section in the spectral analysis of the zenith sky spectra measured by both SYMOCS-VIS and SYMOCS-UV. In Figure 3.11, both a modelled and a measured Ring cross section are shown. Here we see that the spectral features agree very well.

The analysis software includes a procedure for the calculation of the synthetic Ring cross section of appropriate resolution using the algorithm of Chance and Spurr (1997).

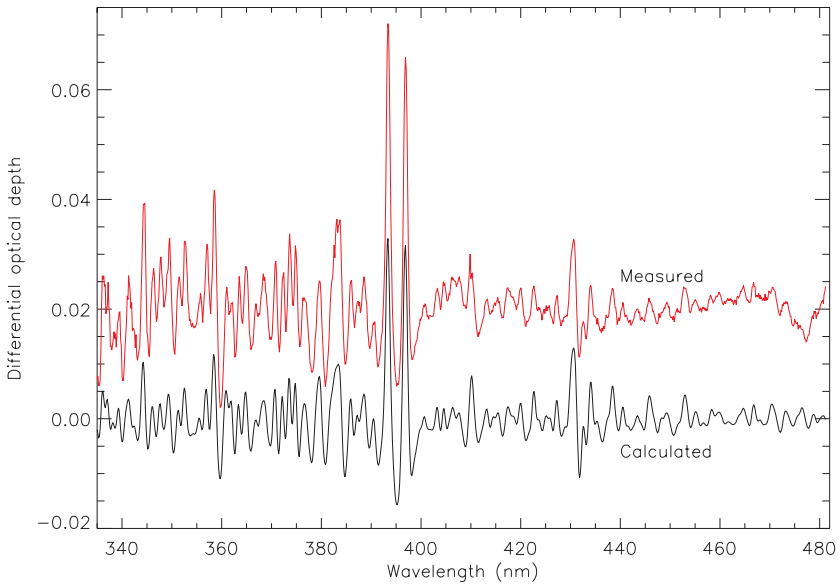

Figure 3.11: A modelled Ring cross section based on rotational Raman scattering calculated by WinDOAS (red) and a measured Ring cross section from 26 March 1996 measured by SYMOCS-VIS (black). An offset of 0.03 is added to the measured cross section for better readability.

3.6 Retrieval of the Compounds

3.6.1 General Considerations

When analysing the spectra, different analysing parameters have to be set for the retrieval of the different compounds. A set of optimised parameters has to be decided upon for each compound. Examples of the parameters include:

- Wavelength region or fitting window,
- Co-absorbing compounds in the chosen wavelength region,
- The quality of the cross sections,
- The cross section temperatures,
- Degree of polynomial to remove the broad-band features due to Rayleigh and Mie scattering, and
- Best suited reference spectrum.

To decide on a wavelength region for a certain species, one has to find compromises between the following

- Using the strongest differential absorption lines of the species to be measured,
- Lowest possible temperature dependency of the cross section of the retrieved compound,
- Lowest possible influence from other strong absorbers in the same wavelength range,
- Avoid correlation between the different cross sections within the chosen wavelength region, and
- Avoid the strongest Fraunhofer.

By narrowing the fitting window, it is possible to exclude absorption features which would otherwise interfere with the absorption lines of the compound to be retrieved. However, this also implies that the degree of non-correlation of the cross sections fitted is reduced. It is therefore of vital importance to choose a fitting window that gives a good degree of non-correlation between the cross sections. Otherwise absorption features of one compound could be interpreted as absorption features of another compound. A proper choice of the fitting window is crucial for an accurate retrieval of relative weak absorbers like BrO and OClO, but also for compounds like O_3 and NO_2. The choice made in this work will be discussed in more detail in this chapter.

Choosing the most appropriate reference spectrum is important for the optimal retrieval of the compound. A good choice can improve the quality of the fit. Normally a reference spectrum that contains little absorption of the absorbing compounds is chosen. Usually a spectrum taken at high sun (e.g. a local noon spectrum) contains little absorption (to benefit from the short light path compared to the twilight spectra). This is possible for compounds that have strong absorption features in atmospheric spectra, such as O_3 and NO_2. The situation is different for measurements of weaker absorbers such as BrO and OClO. As reported by Arpag et al. (1994), Fish et al. (1995), Eisinger et al. (1997) and Aliwell et al. (1997), daily reference spectra taken at a SZA of 80° were used to retrieve BrO and OClO. This to minimise the errors caused by possible

instrumental drift in wavelength that result in increased noise due to larger shift and stretch when aligning the twilight spectra to the reference spectra. During the comparison campaign in OHP daily reference spectra taken at a SZA of 70° was decided upon due to reasons described in Aliwell et al. (2000). Kreher (1996) has reported differential slant columns of BrO where a single reference spectrum for longer measurement periods (typically 3 months) was used. For the retrieval of O_3 and NO_2 we have used a single reference spectrum for longer measurements periods. A spectrum recorded during clear sky conditions is chosen to minimise spectral interference by H_2O and O_4. To use a single reference spectrum for the whole measurement period has not been possible for the retrieval of BrO and OClO due to instrumental drift. However, it has been possible to use a fixed reference spectrum for shorter periods. Normally a daily reference spectrum taken at 80° SZA is used. At Ny-Ålesund and Andøya there are periods in the winter when the SZA never reaches 80°. For these periods a fixed reference spectrum at 80° has been applied in the analysis. The probability for an increase in the retrieval error increases when using a reference spectrum measured another day. This is mainly due to drift in the wavelength calibration that results in larger shift and stretch parameters to be applied to the twilight spectra. This was the case when analysing the spectra from the SYMOCS instruments, but the retrieval error were still well within an acceptable value.

The optical light path traverses through different temperature layers of the atmosphere. The absorption cross sections of several trace gases of atmospheric interest (e.g. O_3, BrO, OClO, NO_2) are very temperature dependent, inducing changes in the absorption features (Platt et al., 1997). This can result in remaining residual features due to imperfect removal. Those artefacts can for example lead to masking of the absorption features of more weakly absorbing species. For the trace gasses NO_2 and O_3 which are strong absorbers, accurate fitting of their cross sections improves the fitting of the weaker absorbers. One should pick the temperature of one of the cross sections that best matches the stratospheric temperature where one finds the bulk of the compound. A way to account for the temperature differences is to use two cross sections measured at different temperatures.

3.6.2 Retrieval of NO_2

NO_2 is best retrieved in the visible wavelength region. The NO_2 spectral absorption is strongly temperature dependent in this spectral region. In Figure 3.12 the NO_2 absorption cross sections at two temperatures are plotted. The differential cross section increases with colder temperatures (e.g. Harder et al., 1997). If a room temperature NO_2 cross section is used in the retrieval of stratospheric NO_2, the NO_2 slant column will be overestimated by approximately 20% (Tørnkvist, 2000). The use of a room temperature cross section give rise to features in the residual which again can reduce the ability to measure absorbers in the same spectral region.

The amplitude of the differential cross section of NO_2 is largest around 440 nm. Different wavelength regions are used to retrieve NO_2 (Roscoe et. al, 1999). There has been an ongoing study in defining the best analysis parameters for the

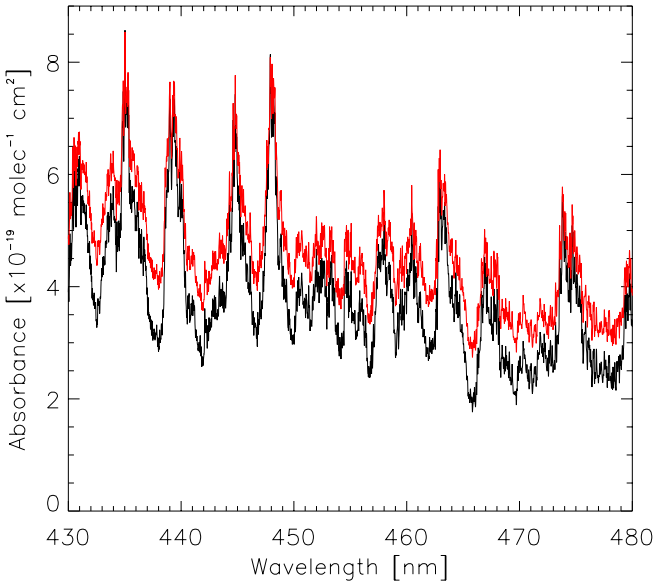

Figure 3.12: The NO_2 absorption cross section at 227 K and 294 K. The NO_2 cross sections are from Harder et al. (1997).

retrieval of NO_2. During the NDSC-campaign at OHP in 1996, NO_2 was retrieved between 415 and 455 nm. Later sensitivity studies showed that the residuals are improved when excluding the Fraunhofer lines around 430 nm from the wavelength region to be fitted. The structure in the residual was systematic and its origin was due to incomplete correction of the Fraunhofer structures. Finally, it was decided to retrieve between 434-480 nm. This change lead to a 1-2% increase in the NO_2 slant columns at 90° SZA. The statistical error in NO_2 retrieved from the DOAS analysis was improved. The retrieval parameters for NO_2 are given in Table 3.4.

Table 3.4: Analysis parameters for the retrieval of NO_2.

Wavelength region	434-480 nm
Absorption cross section	**O_3** Burrows et al. (1999) at 221 K **NO_2** Harder et al. (1997) at 227 K **O_4** Hermans et al. (1999) at 298 K **H_2O** HITRAN database (Rothman et al., 1998) **Ring** Calculated from the WinDOAS software **Offset** Constant
Airmass factors	From IASB-BIRA
Polynomial	Third degree
Smoothing of spectra	none
Wavelength calibration	The Kurucz high resolution Fraunhofer spectrum (Kurucz et al., 1984)
Vertical column	Average between 87° and 91°SZA (AM and PM)
Reference spectrum	Single spectrum taken at high sun
Amount in reference spectrum	Found from Langley plots

For the measurements at Ny-Ålesund spring 1996, two reference spectra were used due to the temperature change in the spectrometer box as described in Chapter 2.8. A reference spectrum measured on 26 March at 76.5° SZA was used for the period 20 February to 28 March. For the period from 1 April to 27 April, a reference spectrum from 26 April at 65.3° SZA was used. In principle one reference spectrum could be used for the whole period, but the error introduced by the shifting and stretching of spectra from the first period onto a reference spectrum from the second period, was significant. By using two different reference spectra the fits, the residuals and the statistical errors were reduced.

3.6.3 Retrieval of O_3

Ozone is usually retrieved in the Chappius band (440-550 nm) when using differential absorption spectroscopy due to the strong temperature dependence of the Huggins band in the UV (300-360 nm). The two bands at two temperatures (221 K and 241 K) are shown separately in Figure 3.13.

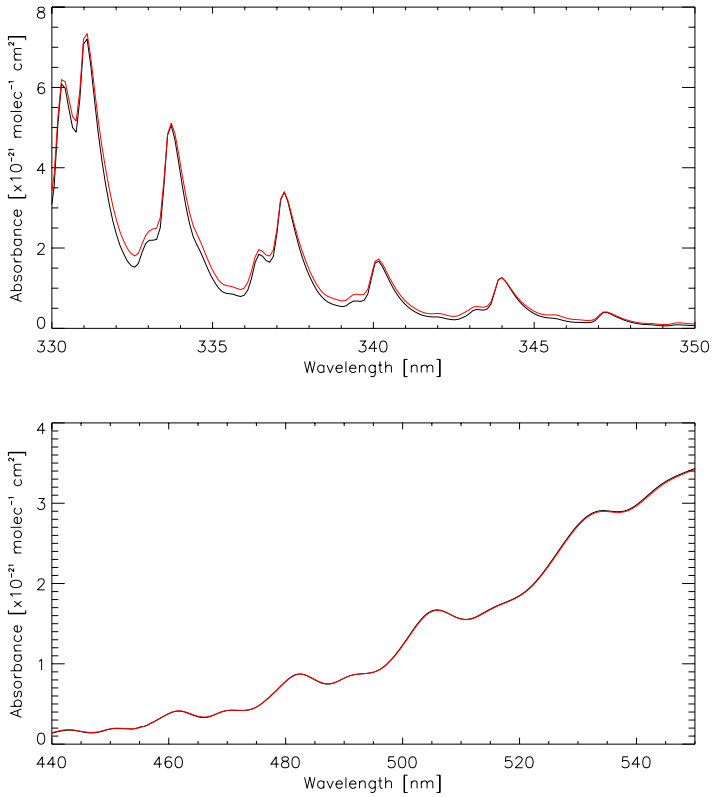

Figure 3.13: The ozone absorption cross section at 221 K and 241 K. The Huggins band is shown in the upper panel while the Chappius band (440-550 nm) is plotted in the lower panel (Burrows et al., 1999).

The strongest differential absorption lines are at 505 and 531 nm, but due to reasons described in Chapter 2.9, ozone was retrieved between 440 and 480 nm when we had only one spectrometer system (measurements from Ny-Ålesund, Longyearbyen and OHP). The development of the additional spectrometer system enabled us to change the O_3 fitting window for SYMOCS-VIS to 470-540 nm. Richter (1997) argues for not including the 505 nm absorption line in the analysis

window due to strong correlation to the water absorption cross section. This has proved not to be a problem when analysing spectra from Ny-Ålesund, probably due to the dry troposphere at this location.

The same reference spectra as for NO_2 were used in the analysis (Chap. 3.6.2). The analysing parameters used for the retrieval of O_3 are summarised in Table 3.5.

Table 3.5: Analysis parameters for the retrieval of O_3.

Wavelength region	440-480 nm (when only one spectrometer system) 470-540 nm (when two spectrometer systems)
Absorption cross section	**O_3** Burrows et al. (1999) at 221 K **NO_2** Harder et al. (1997) at 227 K **O_4** Hermans et al. (1999) at 298 K **H_2O** HITRAN database (Rothman et al., 1998) **Ring** Calculated from the WinDOAS software **Offset** Constant
Airmass factors	Climatological
Polynomial	Third degree
Smoothing of spectra	none
Wavelength calibration	The Kurucz high resolution Fraunhofer spectrum (Kurucz et al., 1984)
Vertical column	Average between 87° and 91°SZA (AM and PM)
Reference spectrum	Single spectrum taken at high sun
Amount in reference spectrum	Found from Langley plots

3.6.4 Retrieval of BrO

The absorption cross section of BrO, shown in Figure 3.4, consists of a series of peaks between 300 and 370 nm with the strongest absorption line at 339 nm. Great care must be taken when deciding on a fitting window for the analysis of BrO due to the high temperature dependence of the ozone cross section combined with strong ozone absorption in the UV (especially for wavelengths shorter than 345 nm). Even small remaining features can mask the absorption features of weak absorbers such as BrO. The correlation between the NO_2 cross section and the BrO cross section for the 345-360 nm range must also be taken into consideration. The wavelength region must be chosen such that the interference from poorly fitted absorbers (e.g. O_3) are minimised combined with sufficient width to ensure anti-correlation between all fitted parameters. Thus BrO is detected from the two absorption lines at 349 and 355 nm. The anti-correlation between NO_2 and BrO cross sections is ensured when choosing the fitting window between 346-359 nm. However, including wavelengths up to 365 nm will strengthen the anti-correlation. The BrO cross section from Wahner et al. (1988) are plotted for the wavelength region chosen for the retrieval of BrO in Figure 3.14.

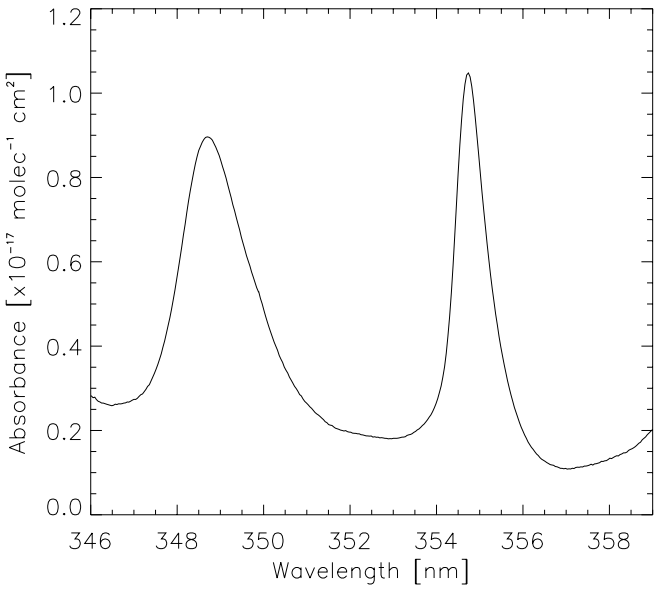

Figure 3.14: The BrO absorption cross section for the 346 to 359 nm wavelength region (Wahner et al., 1988).

The differential slant columns of BrO are sensitive to changes in the fitting window. The effect on the differential slant columns due to variation in the fitting window is shown in Figure 3.15 and Figure 3.16. In Figure 3.15 the results of the sensitivity test performed on spectra measured with the first SYMOCS system (sampling ratio of 6) is shown. A similar test was performed on spectra measured with SYMOCS-UV (sampling ratio of 10), and the results are shown in Figure 3.16. For both cases, the largest change is observed for changes on the short wavelength side. However, the change is less for the SYMOCS spectrometer with the highest sampling ratio. When including wavelengths down to 345 nm, the differential slant columns are reduced by approximately 20% and 12% respectively, at 90° SZA. Aliwell et al. (2000) concluded that the largest effect on the retrieved BrO is seen for the extended fitting window 346-365 nm, which is not consistent with the sensitivity tests performed in this study.

BrO differential slant columns could also be sensitive to the order of the fitted polynomial. In contrast to the general conclusion in Aliwell et al. (2000), sensitivity studies performed on spectra measured by the SYMOCS instruments indicate large sensitivity to the degree of polynomial used. The differential slant columns could increase by as much as 20-30% (around 90° SZA) when increasing the order from 2 to 3. However, since the fitting window is rather narrow, it is important to keep the numbers of fitted variables to a minimum. Therefore a polynomial of second order is used.

Two ozone cross sections at different temperatures are fitted simultaneously in order to approximately account for the effect of having O_3 at different temperatures in the stratosphere. In Figure 3.17 an example of a retrieval of BrO is shown.

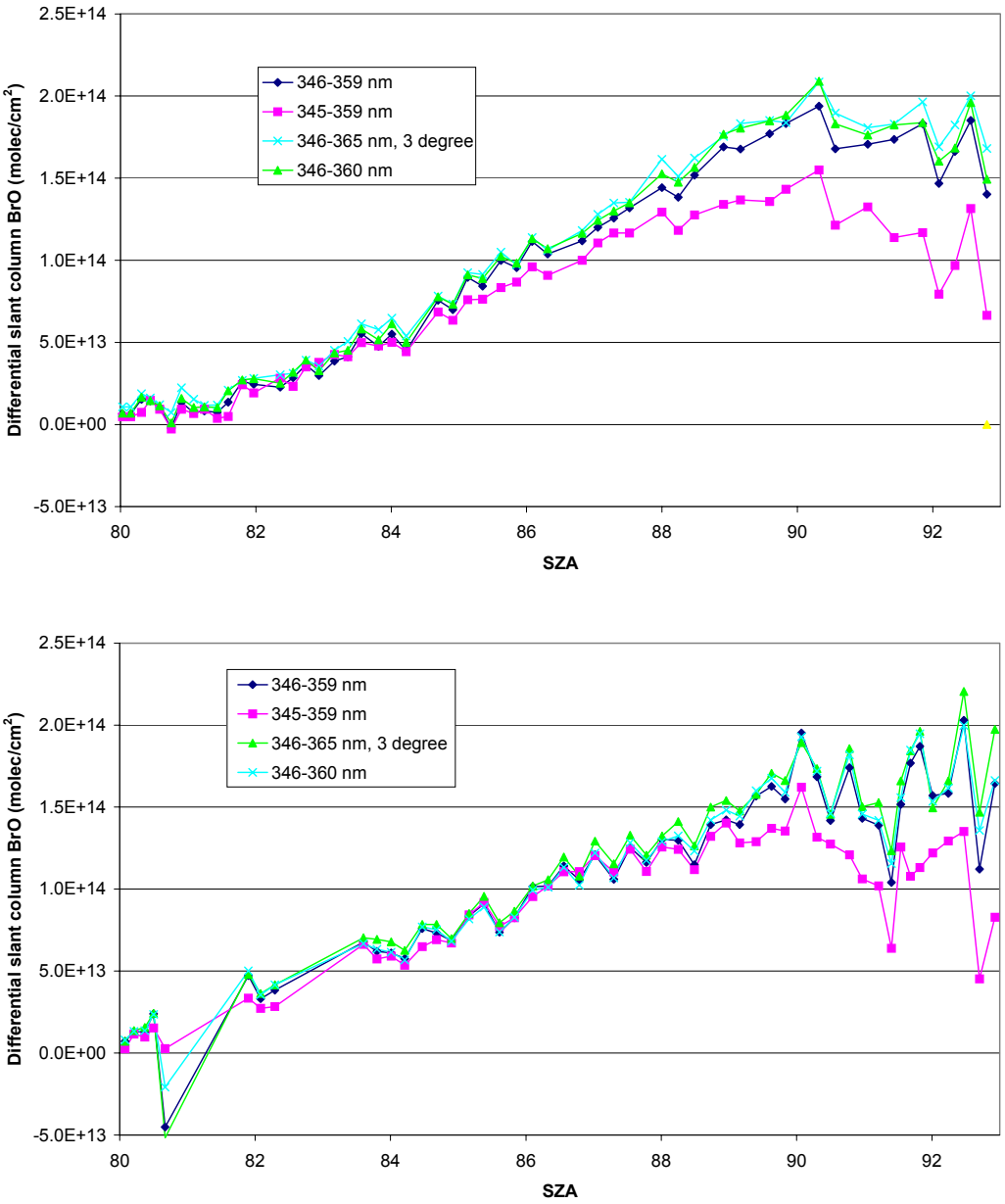

Figure 3.15: Effect on the differential slant columns BrO due to changes in the fitting window. The upper panel shows results from AM 21 March 1997 (Ny-Ålesund), whereas the lower panel shows results from PM the same day. The spectra were measured with SYMOCS when the sampling ratio was 6.

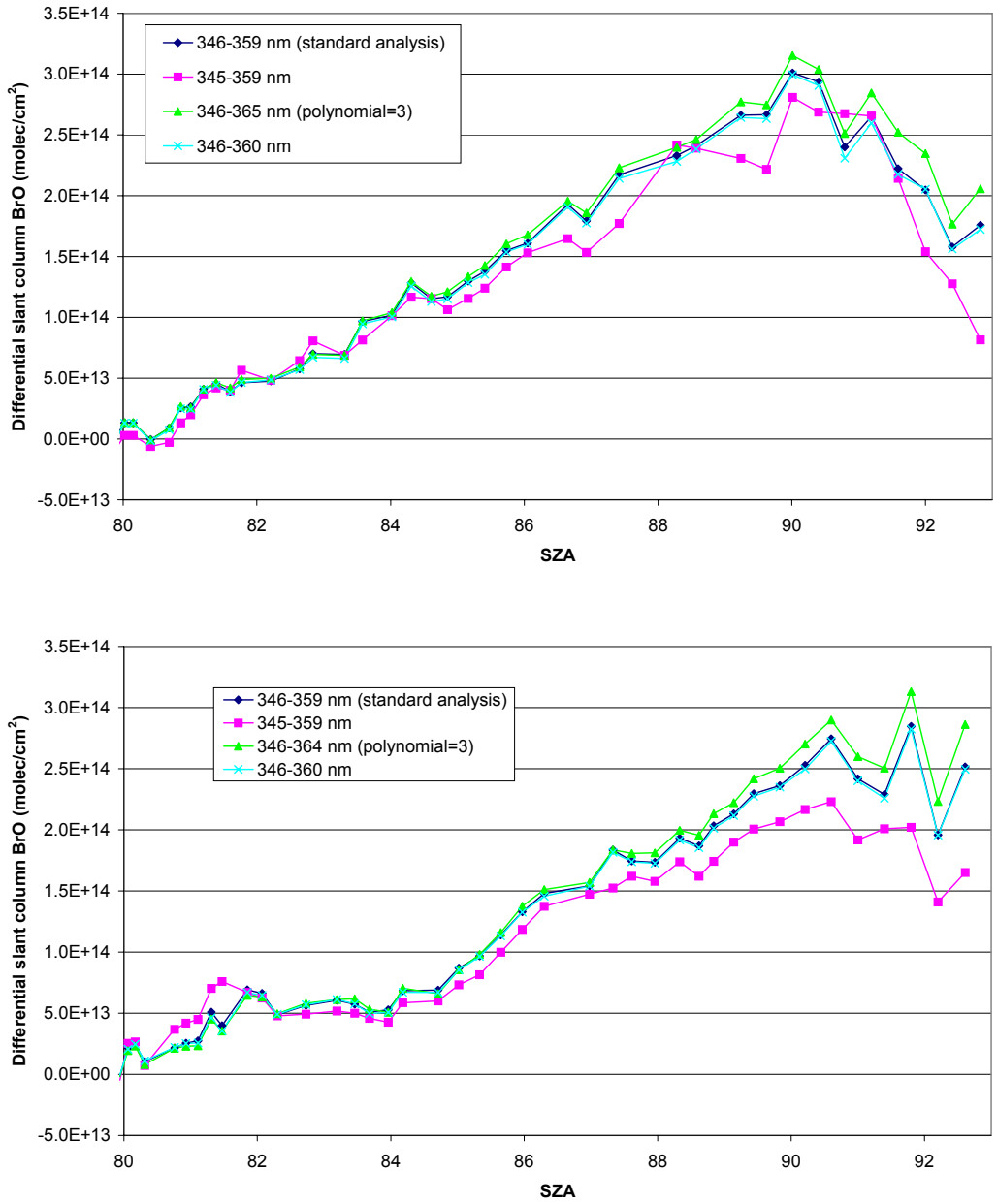

Figure 3.16: Effect on the differential slant columns BrO due to changes in the fitting window. The upper panel shows results from AM 23 February 1999 (Andøya), whereas the lower panel shows results from PM the same day. The spectra were measured with SYMOCS-UV that has a sampling ratio of 10.

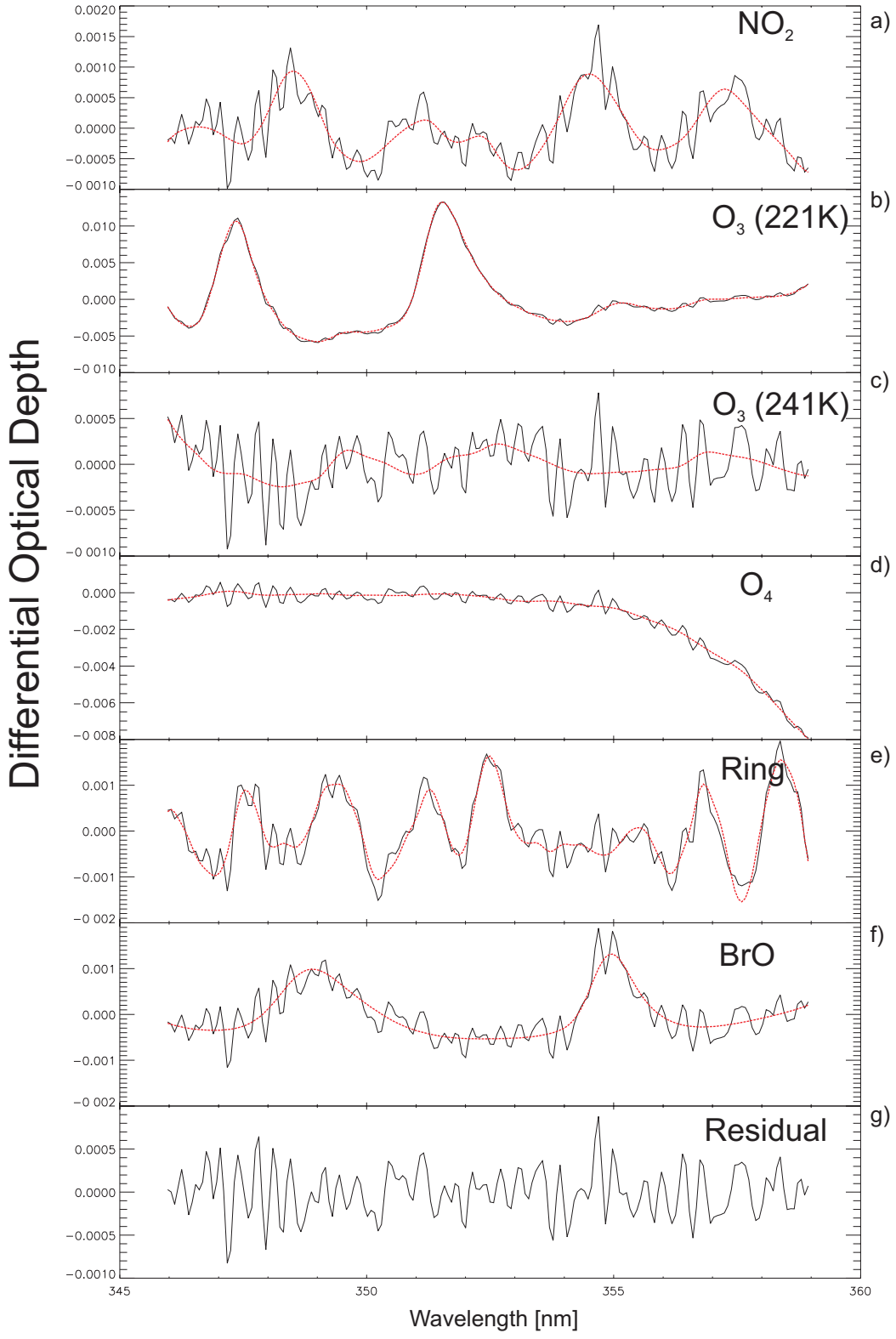

Figure 3.17: The analysis of BrO on the spectrum from 26 February 1999 at a SZA of 89.9° (Andøya). The red curves are the fitted reference cross sections, and the black curves are the measured differential optical depths. The residual is shown in panel g).

Within the project supported by the European Commission (SCUVS-3, 1998), the BrO analysis workshop was held in order to establish a set of recommended analysis scheme for the analysis of BrO. A summary of this work is found in Aliwell et al. (2000). The recommendations were in agreement with conclusions from this work. Therefore, the same analysis scheme has been used for the BrO analysis in this work with exception of the O_4 cross section where we have implemented the latest cross section measured by Hermans et al. (1999) instead of those measured by Greenblatt et al. (1990). The analysis parameters are listed in Table 3.6.

Table 3.6: Analysis parameters for the retrieval of BrO from SYMOCS-VIS and SYMOCS-UV.

Wavelength region	346-359 nm
Absorption cross section	**O_3** Burrows et al. (1999) at 221 K and 241 K (which is orthogonalised to the 221 K cross section) **NO_2** Harder et al. (1997) at 227 K **O_4** Hermans et al. (1999) at 298 K **BrO** Wahner et al. (1988) at 228 K **Ring** Calculated from the WinDOAS software **Offset** Slope
Airmass factors	From IASB-BIRA
Polynomial	Second degree
Smoothing of spectra	Triangular of 3 points (when one SYMOCS system) Odd-even pixel correction (SYMOCS-UV)
Wavelength calibration	The Kurucz high resolution Fraunhofer spectrum (Kurucz et al., 1984)
Vertical column	Found from the slope of the Langley plots
Reference spectrum	Combination of: daily reference spectra (80° SZA) and fixed reference spectrum
Amount in reference spectrum	

3.6.5 Retrieval of OClO

The absorption cross section of OClO, shown in Figure 3.4, consists of a series of peaks between 320 and 425 nm with the strongest absorption lines between 345 and 390 nm. The wavelength range is chosen to exclude the strong O_3 line at 351.5 nm. The ozone line at 359.4 nm is weak and could be included. differential slant columns of OClO vary as function of the chosen wavelength range, but are not as sensitive as BrO. In Figure 3.19 the retrieved differential slant columns of OClO for three different fitting windows are plotted as function of SZA. At 90° SZA, the difference between the 357-385 nm and the 363-395 nm wavelength region is 4%. Between the 357-385 nm and 353-385 nm wavelength region the deviation is 6% this particular evening. It was decided to retrieve OClO between 357-385 nm, which is a compromise between not including the ozone absorption line at 351.5 nm and to include the strongest OClO lines in this region. Some groups analyse OClO between 404 and 424 nm where OClO has some weaker

absorption lines. Sensitivity tests performed on our spectra in this region resulted in significantly higher OClO values and statistical errors which ruled out the possibility of using this wavelength region. The OClO absorption spectrum in the chosen wavelength region is shown in Figure 3.18.

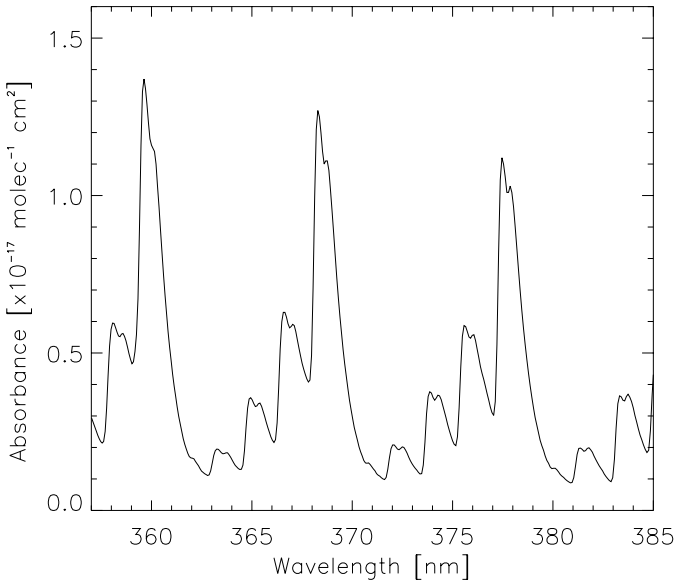

Figure 3.18: The OClO absorption cross section in the 357 to 385 nm wavelength region (Kromminga et al., 1999).

The retrieved BrO amounts are strongly dependent on whether I_0 corrected O_3 cross sections are used or not, as described in Chapter 3.6.4. However, this is not the case for OClO for either O_3 or NO_2. One explanation for this might be that none of the components are strong absorbers in the OClO fitting window as O_3 is in the BrO fitting window.

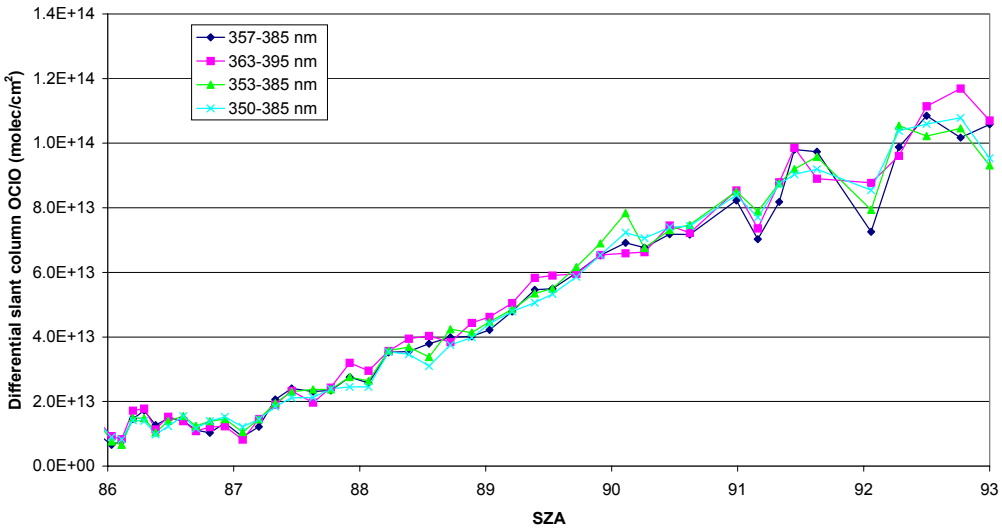

Figure 3.19: An example of how the retrieved OClO differential slant columns change as function of fitting window. The measurements are from Ny-Ålesund 3 March 1996 (PM).

Due to interference between the OClO and the BrO cross section in the chosen wavelength range, the BrO concentration found in the BrO analysis window, is fixed for the analysis of OClO in the OClO window. If the BrO cross section is fitted as all the other cross sections in the OClO window, the BrO lines are not only fitting BrO, but also other structures in the spectra. This is reflected in too large BrO amounts compared to what is retrieved in the BrO window. The retrieved BrO diurnal cycle in the OClO window is not reasonable. The OClO amounts are also dependent on the BrO fitting. By forcing the BrO concentration to the concentration found in the BrO window, the amount of OClO is increased by 10-20% for solar zenith angles between 88° and 92°, and the scatter is reduced. In Figure 3.20 the retrieved OClO amounts where (i) the BrO cross section is fitted as all other cross sections, (ii) the BrO cross section is fitted, but the BrO amount is fixed to the BrO concentration found in the BrO analysis window, and (iii) no BrO is fitted at all, are shown.

Some groups use two NO_2 cross sections at different temperatures for the retrieval of OClO. Sensitivity tests performed on spectra measured with SYMCOS at Ny-Ålesund and Andøya show that it has no or little effect (1-2%) on the retrieved OClO amount (between 88° and 91° SZA) or the residual by including a NO_2 cross section at high temperature.

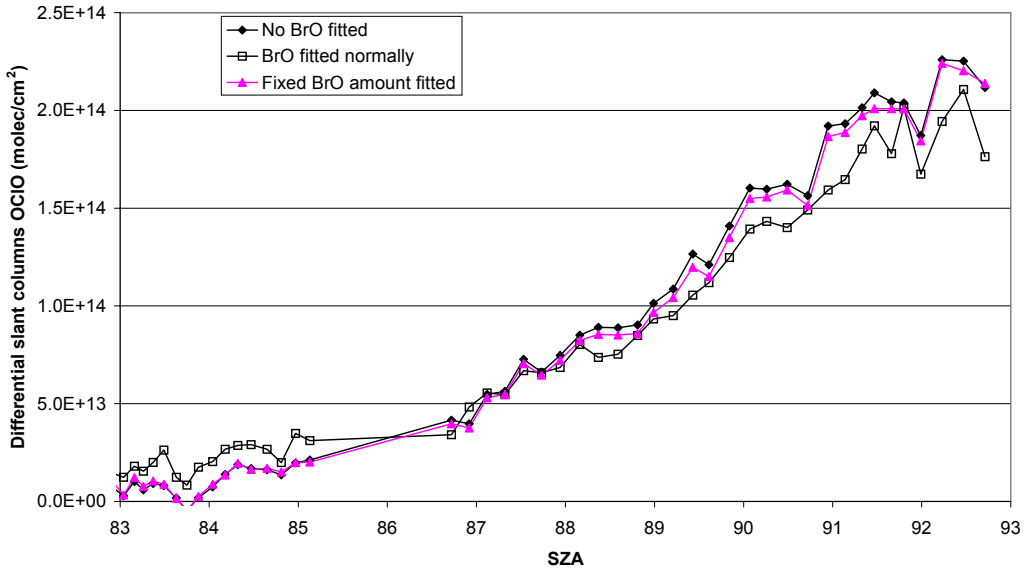

Figure 3.20: Retrieved OClO amounts when (i) no BrO is fitted in the OClO analysis window (black diamonds), (ii) BrO is fitted normally (black open squares) and (iii) BrO is fitted, but the BrO amount is fixed to the concentration found in the BrO analysis window (pink triangles). The example shown here is from PM 12 March 1997 (Ny-Ålesund).

Table 3.7 summarises the cross sections and other parameters used in the analysis of OClO. An example of a retrieval of OClO is plotted in Figure 3.21.

Table 3.7: Analysis parameters for the retrieval of OClO.

Wavelength region	357-385 nm
Absorption cross section	**O_3** Burrows et al. (1999) at 221 K **NO_2** Harder et al. (1997) at 227 K **O_4** Hermans et al. (1999) at 298 K **BrO** Wahner et al. (1988) at 228 K **OClO** Kromminga et al. (1999) at 213 K **Ring** Calculated from the WinDOAS software **Offset** Slope
Airmass factors	-
Polynomial	Second degree
Smoothing of spectra	Triangular of 3 points (when one SYMOCS system) Odd-even pixel correction (SYMOCS-UV)
Wavelength calibration	The Kurucz high resolution Fraunhofer spectrum (Kurucz et al., 1984)
Vertical column	-
Reference spectrum	Combination of: Daily reference spectra (80° SZA) and Fixed reference spectrum
Amount in reference spectrum	-
Comment	When fitting BrO in the OClO window, the BrO amount is fixed to the amount found in the BrO window.

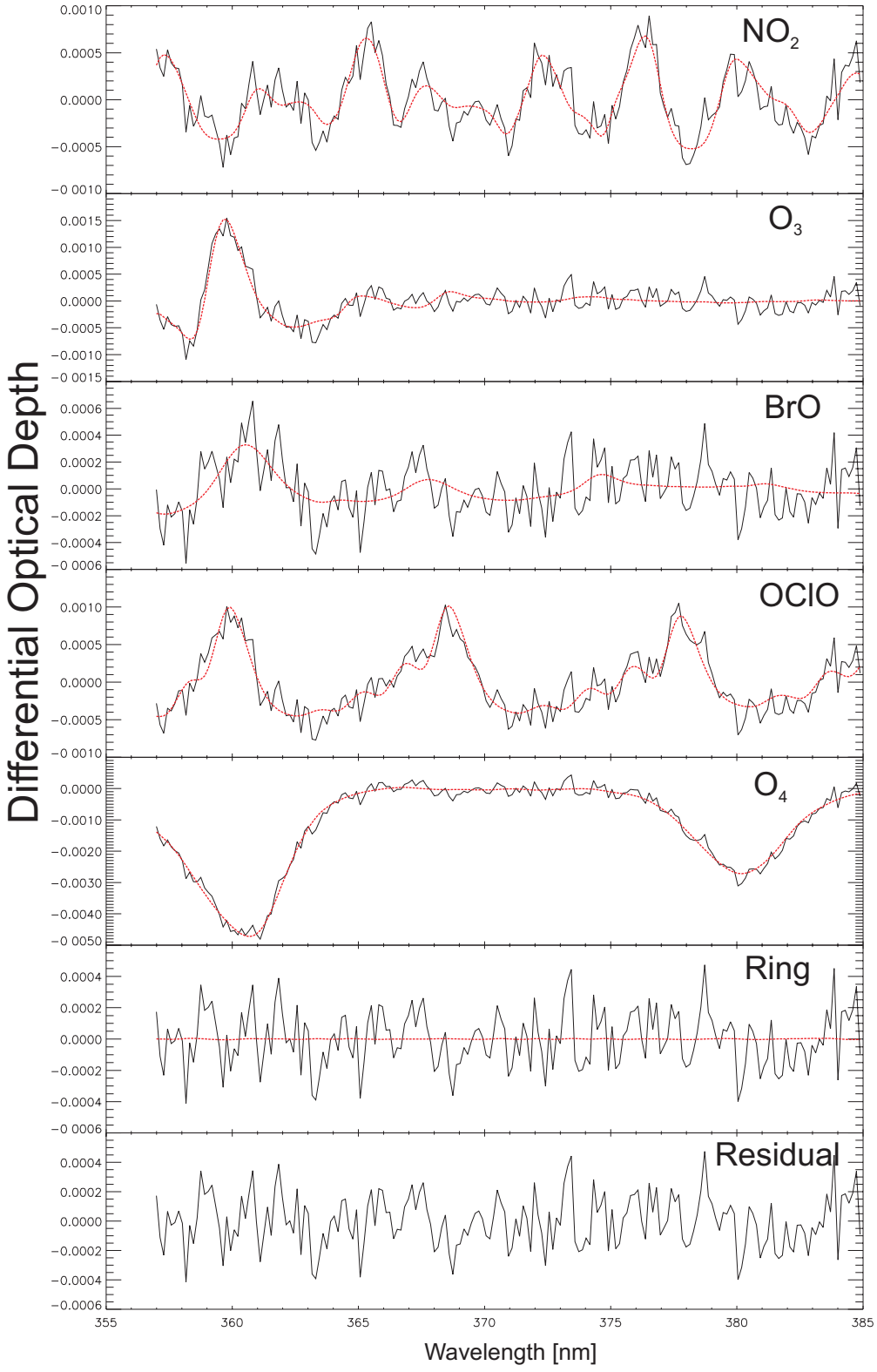

Figure 3.21: The analysis of OClO on the spectrum from 16 March 1997 at a SZA of 90.3° (Ny-Ålesund). The red curves are the fitted reference cross sections, and the black curves are the measured differential optical depths. The residual is shown in lowest panel.

3.7 Conversion from Differential Slant Columns to Vertical Columns

With a zenith viewing spectrometer, the quantity one measures is the slant column due to the slant path that the light has traversed. The output from the spectral analysis is the measured line-of-sight amount of each compound fitted minus the amount in the reference spectrum (differential slant column). It is, however, of interest to convert the measured slant column to a vertical column of the absorber, because the vertical column shows the diurnal variation in the concentration more precisely. In addition, the vertical column is often a better quantity to use when comparing measurement with model results and satellite observations. One way to calculate the vertical column, *VC*, is by using the equation

$$VC = \frac{DSCD + REF}{AMF}, \qquad \textit{Eq. 3.17}$$

where D*SCD* is the differential slant column, *REF* is the amount in the reference spectrum and *AMF* is the so-called airmass factor (see Chapter 3.7.1). In other words, the vertical column is dependent on a proper estimation of the reference amount and the calculated airmass factors used.

Rewriting Eq. 3.17, we see that the vertical column could also be found as the slope in the following equation

$$DSCD = VC * AMF - REF\ . \qquad \textit{Eq. 3.18}$$

Plotting the differential slant columns as a function of the airmass factor, we obtain a Langley plot. It is common to use Langley plots to find the reference amount (Chapter 3.7.2), but as will be described in Chapter 3.7.4, Langley plots are also used to calculate vertical columns of a compound.

3.7.1 Airmass factor

The airmass factor (*AMF*) is defined by

$$AMF(\lambda,\theta) = \frac{\text{slant column}(\lambda,\theta)}{\text{vertical column}(\lambda,\theta)}. \qquad \textit{Eq. 3.19}$$

The AMF is the effective enhancement in optical path through the atmosphere relative to the vertical path. In fact, the AMF is the enhancement factor in the stratosphere since the AMF in the troposphere is unity when observing the scattered light from zenith near twilight (except during snowfall or thick clouds, Erle et al., 1995). For direct sun (or moon or star) measurements, the calculation of AMF is straightforward. For scattered light observations, the computation becomes more complex since the light traverses a range of paths through the absorbing layer. For these calculations one needs a radiative transfer model where the vertical distribution of the absorber of interest and of constituents that influence the light path through the atmosphere have to be assumed. The airmass factor is influenced by the solar zenith angle, the wavelength of light, the profile of the absorbing species, the temperature and pressure profiles and the presence and characteristics of aerosols. The airmass factors used for converting ozone differential slant columns to vertical columns in this work were calculated by

using the Discrete Ordinate Radiative Transfer (DISORT) method (Stamnes et al., 1988; Dahlback et al., 1991). The airmass factors were calculated using ozone, temperature and pressure profiles measured by ptu-sondes at Ny-Ålesund. Hereby the seasonal variation in the airmass factors is accounted for. A detailed description of the calculations is found in Høiskar et al. (1997).

The airmass factors used for the determination of total column NO_2 were calculated at IASB-BIRA by means of a single scattering model (simple ray tracing algorithm) using the AFGL[7] subarctic winter atmosphere and the standard AFGL NO_2 profile, under clear sky conditions (no aerosols). No seasonal dependence is taken into account, and the same set of airmass factors is used throughout the year.

Airmass factors for BrO and OClO have not been calculated on a regular basis as far we as know. When calculating AMFs for species that can exhibit strong diurnal variations (NO_2, BrO and OClO), the chemical enhancement effect should be accounted for. The effect arises when the concentration varies along the light path during changes in the local SZA. However, a preliminary study by Kreher (1996) indicated that sunrise and sunset BrO vertical columns and sunrise OClO vertical columns measured at SZA < 92° as well as evening OClO vertical columns at SZA < 90° can be retrieved reasonably well without inclusion of chemical enhancement. The AMFs used in the first retrieval of BrO vertical columns reported in this work were calculated without chemical enhancement. The calculations were performed by using the DISORT model. A standard BrO profile with no BrO below 13 km, 14 ppt above 20 km and a BrO mixing ratio increasing linearly between 13 and 20 km were used as input in the model calculations (Hendrick, personal communication).

The airmass factors for O_3, NO_2 and BrO used for converting differential slant columns to vertical columns are listed in Appendix 1.

3.7.2 Determination of the Amount in the Reference Spectrum

The amount in the reference spectrum is found from a Langley plot which is the plotting of the differential slant column amounts *vs*. the AMF according to Eq. 3.16. REF is found as the intercept at zero AMF. An example of a Langley plot is shown in Figure 3.22.

For gases with little or no diurnal variation, such as O_3, the observed differential slant columns should follow a straight line when plotted as a function of the corresponding AMF. If the constituent amount has a systematic diurnal variation such as NO_2 and BrO, the Langley plot will be curved, and a standard Langley plot method cannot therefore be expected to give satisfactory results. However, a modified form of a Langley plot (Lee et al., 1994) are used to derive the amount of NO_2 in the reference spectrum. Lee et al. (1994) implemented a modified form of Langley plot where assumptions about the relationship of the actual diurnal variation of NO_2 is taken into account. In this work a subjective determination of the reference amount has been used. A Langley plot is combined with a subjective

[7] Air Force Geophysics Laboratory

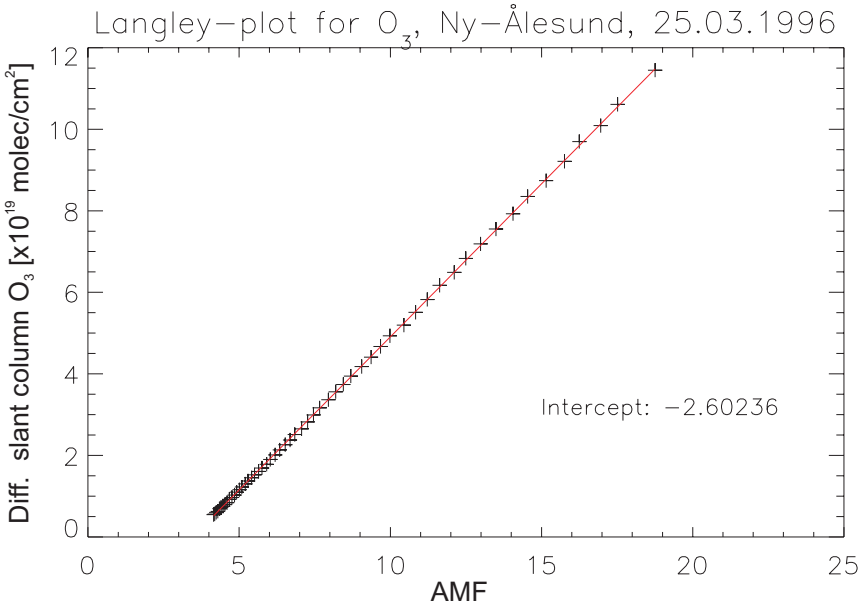

Figure 3.22: Example of a Langley plot for ozone. The differential slant columns are measured 25 March 1996 at Ny-Ålesund.

examination by eye examination of the shape of the diurnal variation of NO_2 is used. The subjective method is based on a monotonic increase of NO_2 during the day due to photolysis of N_2O_5. The method of Lee and co-workers is more consistent than the subjective method since it is defined in the calculations instead of in the mind of the operator. Vertical columns are plotted and judged for each day for different reference amount. In Figure 3.23 the calculated diurnal variation of vertical columns NO_2 is plotted for three different reference amounts. The black crosses represent an overestimated amount in the reference spectrum, whereas the black stars represent an underestimated reference amount. The red curve represents a "true" of the diurnal variation, and corresponds to a correct reference amount that would be used for the calculations. The 'first guess' is the intercept obtained from a normal Langley plot.

For ozone, measurements between 70° and 91° SZA with statistical errors less than 3% are used in the Langley plot. For NO_2 only PM measurements between 80 and 91° SZA are used in the Langley plot to estimate the 'first guess'-amount in the background spectrum since the NO_2 amounts are supposed to vary less with SZA in the evening twilight. Only measurements with a statistical error less than 10% are included.

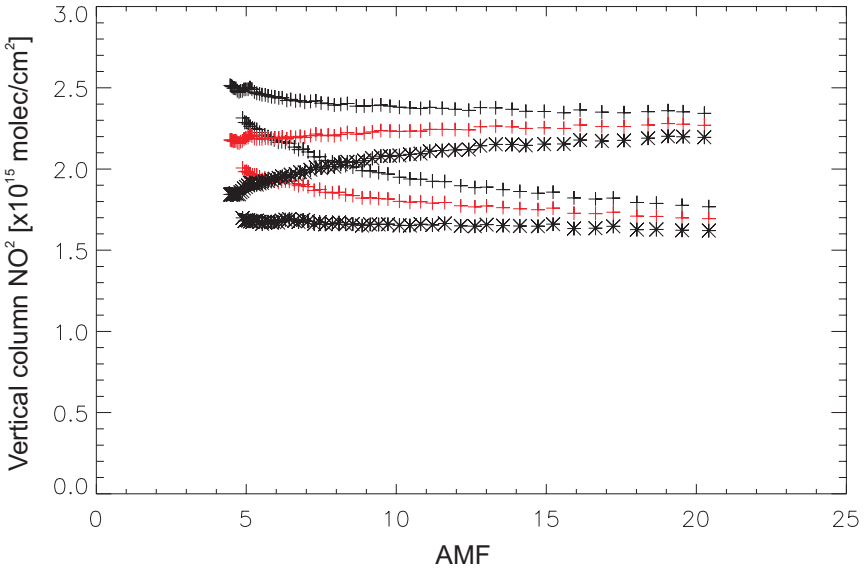

Figure 3.23: Example of the shape of the diurnal variation of NO_2 when using different reference amounts in Eq. 3.15. The vertical columns are from 22 March 1996 (Ny-Ålesund). The red curve is typical for a diurnal variation that would be chosen as the "right" one. The black stars are representative of a shape where the reference amount is underestimated, and the black crosses are representative of a shape where the reference amount is overestimated.

3.7.3 Vertical columns of ozone and NO_2

Vertical column amounts are usually averaged over a suitable range of solar zenith angles to obtain daily mean values or morning and evening mean values. The precision and accuracy of the vertical columns are optimal around 90° SZA. Van Roozendael et al. (1994) reported that errors in mean values of O_3 and NO_2 are minimised by using data recorded between 87° and 91° SZA. Differential slant columns with a retrieval error less than 3% for ozone and 10% for NO_2 are used in the weighted-mean calculations.

3.7.4 Vertical columns of BrO

The first reported BrO and OClO vertical columns from a ground-based instrument are found in Kreher (1996). Due to the inherent difficulty with such calculations, the determination of vertical columns BrO from ground-based spectrometers has only been performed on a test basis. Two factors are necessary for converting differential slant columns to vertical columns, i.e. calculations of airmass factors (Chap. 3.7.1) and estimates of the amount in the reference spectrum. For the computations of the airmass factors the vertical profile of the compound is needed. Profile measurements show relatively large variations (e.g. Pundt et al., 2000**)**. The concentration of BrO changes rapidly around twilight. However, if one assumes that BrO is photochemically stable at SZAs less than e.g. 80°, Langley plots including measurements up to 80° can be used to derive the vertical column of BrO. Preliminary studies show, however, that the calculated vertical BrO columns highly depends on which SZAs that have been included in the Langley-plot. In Figure 3.24 vertical columns of BrO derived

using the Langley–plot approach for different SZA ranges are shown. The red triangles represents vertical columns retrieved when including measurements between 70° and 85° SZA. This curve corresponds to twilight conditions. The green squares represent vertical columns derived when including measurements between 50° and 80° SZA, and the blue diamonds represent vertical columns when only including measurements between noon and 75° SZA. Different parts of the diurnal cycle are sampled.

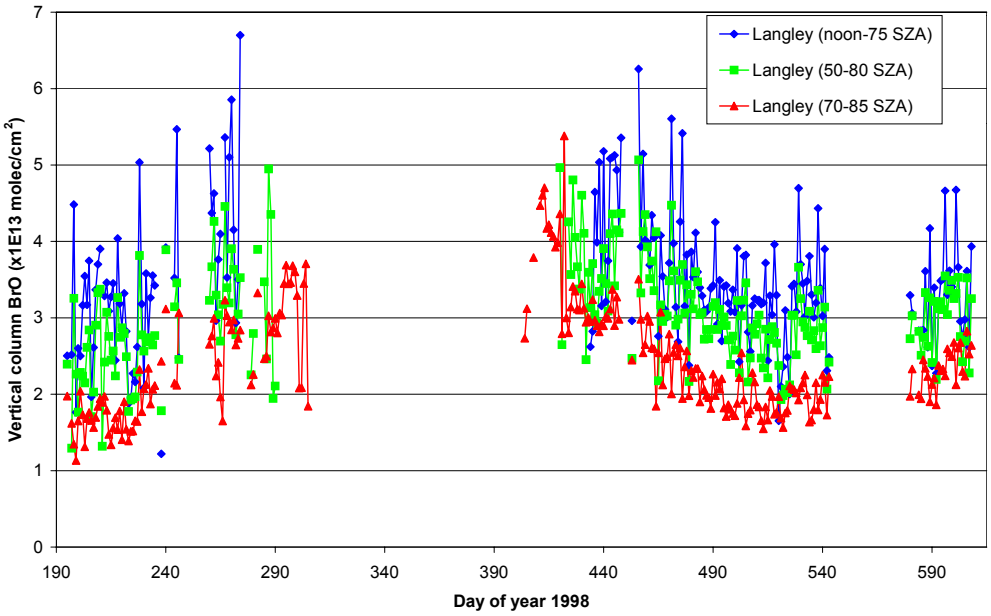

Figure 3.24: Vertical columns of BrO above Andøya for the period July 1998 to August 1999. The different series are derived by including different SZA ranges in the Langley plots.

Spectra from April, May and June 1999 were analysed with different fixed reference spectra (at 55°, 70° and 80° from 2 May 1999). In Table 3.8 the vertical columns calculated by using the three different reference spectra are shown for some selected days. The consistency in the vertical columns retrieved by using three different reference spectra, support that the method is reliable. However, these are only preliminary results, and the method has to be further tested and verified. The method has not been tried for OClO yet.

Table 3.8: Vertical columns of BrO for some selected days from the period April to June 1999 at Andøya using three different reference spectra.

Reference spectrum at	Day 119	Day 125	Day 138
55°SZA	3.38	3.76	3.25
70°SZA	3.41	3.62	3.10
80°SZA	3.45	3.60	3.13

3.8 Error sources and estimates

In this chapter the different sources of errors will be discussed and the magnitude of the total error for the different constituents will be estimated. The errors can be divided into either random or systematic. Measurement errors are mainly systematic errors and are associated with the instrument, the spectral analysis, the determination of the amount in the reference spectrum and the airmass factor calculations. The standard deviations of the least-squares fit from the retrieval of the differential slant columns gives an indication of the quality of the fits, that is the difference between the measured spectrum and the calculated spectrum. This error estimation include errors introduced by spectral alignment (i.e. shifting and squeezing) of the twilight spectrum onto the reference spectrum, to small changes in the instrumental resolution and ILS and to detector noise. For ozone the statistical fit error at 90° SZA is less than 1% and for NO_2 less than 4%. The retrieval error for BrO is reduced both in magnitude and scatter when measured with SYMOCS-UV compared to the first SYMOCS instrument. The retrieval error is also less in winter than in summer since the differential slant columns of BrO is higher in winter. BrO measured with SYMOCS-UV has a statistical error at 90° SZA of 10-20% whereas BrO measured with the first SYMOCS instrument had a statistical fit error that varied between 15-40%. The retrieval error for OClO is more or less the same for both instruments and varies between 5-25%. The detection limits are estimated from the residuals of the fits. For BrO the detection limit was estimated to $5 \cdot 10^{13}$ molec/cm^2 for the first SYMOCS instrument and $3 \cdot 10^{13}$ molec/cm^2 for SYMOCS-UV. For OClO the detection limit is estimated to $5 \cdot 10^{13}$ molec/cm^2. The detection limit of NO_2 and O_3 are approximately $4 \cdot 10^{14}$ molec/cm^2 and $7 \cdot 10^{14}$ molec/cm^2 respectively.

An extensive error analysis was performed by Van Roozendael et al. (1994) and Richter (1997). The uncertainty in the absorption cross section introduces a systematic contribution to the total error. The error in the O_3 cross section used (Burrows et al., 1999) is less than 3%. The uncertainty in the NO_2 cross section from Harder et al. (1997) is estimated to 4%. Wahner et al. (1988) report of an uncertainty in the BrO cross section of approximately 7%. The OClO cross section has an uncertainty of less than 8% (Kromminga et al., 1999).

Other sources of error, such as a baseline offset caused by stray light or incorrect subtraction of dark current, or inaccuracies in the wavelength calibration cause systematic features in the observed residuals. In Richter (1997) results from a sensitivity study performed on synthetic spectra on the influence of a inaccuracy in the wavelength calibration of absorption cross sections are found. An inaccurate wavelength calibration in ozone has the largest effect of the analysis of ozone and BrO. For NO_2 and OClO, the NO_2 cross section has the largest influence. The results are listed in Table 3.9 under “Error due to bad wavelength calibration in cross section”.

The uncertainty in the retrieved BrO and OClO differential slant columns are relative to the standard analysis case (Table 3.6 and Table 3.7) in order to illustrate the change caused by changing the analysis. The sensitivity tests, which are described in Chap. 3.6.4 and Chap. 3.6.5, should be seen as an indication of the areas of concern for the analysis rather than absolute error estimates. The main

error sources include wavelength interval for analysis, the use of I_0-corrected cross sections or not, the degree of the polynomial used to remove the broad-band features, and offset corrections.

There are uncertainties coupled to the calculation of the airmass factors as well. The airmass factors used for the conversion of slant column O_3 to vertical column O_3 are calculated by using pressure, temperature and ozone profiles measured by sondes. The day-to-day variation of the true airmass factors introduce an uncertainty in the daily ozone values of approximately 1.5% (Høiskar et al., 1997). The seasonal dependence in pressure temperature and NO_2 profile are not taken into account in the calculations of the airmass factors used for NO_2. Recent studies (Høiskar et al., 2000; Lambert et al., 2000) indicate that the error introduced by not accounting for a seasonal variation in pressure, temperature and NO_2 profile, and a diurnal variation in the NO_2 profile is approximately 8%.

The total error budget is listed in Table 3.9. The I_0-correction term is not included in the total error since this is an effect which is corrected for.

Table 3.9: Error budget for O_3 and NO_2 vertical columns and differential slant columns of BrO and OClO measured with the SYMOCS spectrometers.

Source of error	**O_3**	**NO_2**	**BrO**	**OClO**
Statistical fitting error	< 1%	<4%	10-40%	5-25%
Absorption cross section	3%	4%	7%	< 8%
Error due to bad wavelength calibration in cross section	< 1%	< 5%	< 10%	<10%
Wavelength interval		< 1.5%	< 20%	6%
Degree of polynomial			< 25%	
Offset correction	< 0.5%	< 2%	< 15%	< 10%
I_0-correction			25%	
Fixing the BrO amount, or not, for the retrieval of OClO				< 20%
Amount in reference spectrum	2%	4%		
Airmass factor	1.5%	8%		
Total	**< 4.2%**	**< 12%**	**< 39-55%**	**< 27-36%**

4 Summary

This report describes the development of two ground-based UV-visible spectrometers for measurements of compounds (O_3, NO_2, BrO and OClO) in the stratosphere. From 1995-1997 only one instrument measured all four compounds from Ny-Ålesund and Longyearbyen. In 1998 another spectrometer system was developed to increase the quality of the measurements. SYMOCS-VIS (System for Monitoring Compounds in the Stratosphere) measures O_3 and NO_2, whereas SYMOCS-UV measures BrO and OClO. The SYMOCS-VIS spectrometer has a

wavelength resolution of 0.9 nm and a sampling ratio of 6. SYMOCS-UV has a slightly better wavelength resolution (0.6 nm) and a sampling ratio of 10.

The DOAS technique (Differential Optical Absorption Spectroscopy) is used for analysing the measured spectra. An analysis program developed at IASB-BIRA has been employed. The establishment of the different analysis schemes for the retrieval of the differential slant columns for the four compounds is described in this report. For NO_2 and O_3 the differential slant columns are converted to total vertical columns. For both NO_2 and O_3 a fixed reference spectrum is used in the analysis, and the amount in the reference spectrum is found from Langley plots. The calculation of vertical columns of BrO has been performed on a test basis.

NO_2 is retrieved in the wavelength region between 434 nm and 480 nm. Currently a low-temperature NO_2 cross section measured by Harder et al. (1997) is used. The total error in total column NO_2 is estimated to be less than 12%. Ozone is currently retrieved between 470 nm and 540 nm, but was retrieved between 440 nm and 480 nm when only one spectrometer system was in operation (1995-1997). The ozone cross section was measured at 221 K (Burrows et al., 1999). The total error in total column ozone is estimated to be less than 4.2%.

BrO is retrieved between 346 nm and 359 nm. BrO absorbs in the UV wavelength region where O_3 is a strong absorber. To be able to remove the absorption due to O_3 as completely as possible, two ozone cross sections at two different temperatures (221 K and 241 K) are used in the analysis for BrO. It is also important to use I_0-corrected O_3 cross sections in the analysis to remove the ozone absorption structure in the analysis window properly.. The total uncertainty in the retrieved differential slant column BrO is estimated to vary between 39 and 55%.

OClO is retrieved in the 357-385 nm wavelength region. The OClO absorption line overlaps with a BrO absorption line. The BrO concentration found in the BrO analysis window is therefore fixed for the retrieval of OClO. The total error in differential slant column OClO is estimated to vary between 27 and 36%.

5 References

Aliwell, S.R. and Jones, R.L. (1997) Mid-latitide observations of the seasonal variation of BrO 1. Zenith-sky measurements. *Geophys. Res. Lett., 24*, 10, 1195-1198.

Aliwell, S.R., Johnston, P.V., Richter, A., Van Roozendael, M., Wagner, T., Arlander, D.W., Burrows, J.P., Fish, D.J., Jones, R.L., Tørnkvist, K.K., Lambert, J.-C., Pfeilsticker, K. and Pundt, I. (2000) Analysis for BrO in zenith-sky spectra – an intercomparison exercise for analysis improvement. To be submitted to *J. Geophys. Res.*

Arpag, K.H., Johnston, P.V., Miller, H.L., Sanders, R.W. and Solomon, S. (1994) Observations of the stratospheric BrO column over Colorado, 40°N. *J. Geophys. Res., 99*, 8175-8181.

Burrows, J.P., Richter, A., Dehn, A., Deters, B., Himmelmann, S. (1999) Atmospheric remote-sensing reference data from GOME - 2. Temperature-dependent absorption cross-sections of O_3 in the 231-794 nm range. *J. Quant. Spectrosc. Radiat. Transfer*, *61*, 4, 509-517.

Chance, K. and Spurr, R. (1997) Ring effect studies: Rayleigh scattering, including molecular parameters for rotational Raman scattering, and the Fraunhofer spectrum. *Appl. Optics*, *36*, 5224-5230.

Conde, M., Greet, P. and Jacka, F. (1992) The ring effect in the sodium D2 Fraunhofer line of day skylight over Mawson, Antarctica. *J. Geophys. Res., 97,* 11561-11565.

Dahlback, A. and Stamnes, K. (1991) A new spherical model for computing the radiation field available for photolysis and heating at twilight. *Planet. Space Sci., 39,* 671-683.

Eisinger, M., Richter, A., Ladstatter-Weissenmayer, A. and Burrows, J.P. (1997) DOAS zenith sky observations: 1.BrO measurements over Bremen (53°N) 1993-1994. *J. Atmos. Chem., 26*, 93-108.

Erle, F, Pfeilsticker, K. and Platt, U. (1995) On the influence of tropospheric clouds on zenith-scattered-light measurements of stratospheric species. *J. Geophys. Lett., 22,* 2725-2728.

European Commission (1997) European research in the stratosphere. The contribution of EASOE and SESAME to our current understanding of the ozone layer. Luxembourg, Office for Official Publications of the European Communities (EUR 16986).

Fish, D.J., Jones, R.L. and Strong, E.K. (1995) Strong Mid-latitude observations of the diurnal variation of stratospheric BrO. *J. Geophys. Res., 100*, 18863-18871.

Grainger, J.F. and Ring, J. (1962) Anomalous Fraunhofer line profiles. *Nature, 193*, 762.

Greenblatt, G.D., Orlando, J.J., Burkholder, J.B. and Ravishankara, A.R. (1990) Absorption measurements of oxygen between 330 and 1140 nm. *J. Geophys. Res., 95*, 18577-18582.

Harder, J.W., Brault, J.W., Johnston, P.V., Mount, G.H. (1997) Temperature dependent NO_2 cross sections at high spectral resolution. *J. Geophys. Res*., *102*, 3,862-3,879.

Hermans, A., Vandaele, C., Carleer, M., Fally, S., Colin, R., Jenouvrier, A., Coquart, B. and Mérienne, M.-F. (1999) Absorption cross-sections of atmospheric constituents: NO_2, O_2, and H_2O. *Environ. Sci. & Pollut. Res., 6,* 151-158.

Hofmann, D., Bonasoni, P., De Maziere, M., Evangelisti, F., Giovanelli, G., Goldman, A., Goutail, F., Harder, J., Jakoubek, R., Johnston, P., Kerr, J., Matthews, W.A., McElroy, T., McKenzie, R., Mount, G., Platt, U., Pommereau, J.-P., Sarkissian, A., Simon, P., Solomon, S., Stutz, J., Thomas, A., Van Roozendael, M. and Wu, E. (1995) Intercomparison of UV/visible spectrometers for measurements of stratospheric NO_2 for the network for the detection of stratospheric change. *J. Geophys. Res., 100*, 16,765-16,791.

Høiskar, B.A.K., Vaughan, G., Dahlback, A., Braathen, G.O., Pommereau, J.-P., and Kivi, R. (1997) Interpretation of ozone measurements by ground-based visible spectroscopy – a study of the seasonal dependence of airmass factors for ozone based on climatology data. *J. Quant. Spectrosc. Radiat. Transfer, 57*, 4, 569-579.

Høiskar, B.A.K. (1997) Evaluation and interpretation of spectroscopic measurements in the stratosphere. Doctoral thesis. The University of Oslo.

Høiskar, B.A.K., Fløisand, I. and Tørnkvist, K.K. (2000) Seasonal variation in air mass factors for NO_2. To be in Proc. 5th European Symposium on Stratospheric Ozone Research (Saint-Jean-de-Luz, Basque, France, Sept. 27 September-1 October, 1999).

Johnston, P.V. (1996) Making UV/Vis cross sections, reference Fraunhofer and synthetic spectra. Unpublished document.

Kreher, K. (1996) Spectroscopic measurement of atmospheric OClO, BrO and NO_2 and their relation to Antarctic ozone depletion. Doctoral thesis. The University of Heidelberg.

Kromminga, H., Voigt S., Orphal J. and Burrows J.P. (1999) UV-visible FT spectra of OClO at atmospheric temperatures. In: *Proceedings of the 1st European Symposium on Atmospheric Measurements from Space*. (ESA Special Publication).

Kurucz, R.L., Furenlid, I., Brault, J. and Testerman, L. (1984) Solar flux atlas from 296 nm to 1300 nm. (National Solar Observatory Atlas No. 1).

Lambert, J.-C., Van Roozendael, M., Sarkissian, A., Goutail, F., Müller, J.-F., Pommereau, J.-P. and Russel, J.M. (2000) A climatology of NO_2 profile for improved air mass factors for ground-based vertical column measurements. To be in Proc. 5th European Symposium on Stratospheric Ozone Research (Saint-Jean-de-Luz, Basque, France, Sept. 27 September-1 October, 1999).

Lee, A.M., Roscoe, H.K., Oldham, D.J., Squires, J.A.C., Sarkissian A., Pommereau, J.-P. and Gardiner, B.G. (1994) Improvements to the accuracy of measurements of NO_2 by zenith-sky visible spectrometer. *J. Quant. Spectrosc. Radiat. Transfer, 52*, 5, 649-657.

Mount, G., Sanders, R.W. and Brault, J.W. (1992) Interference effects in Reticon photodiode array detectors. *Appl. Opt., 31*, 7.

Penndorf, R. (1957) Tables of the refractive index for standard air and the Rayleigh scattering coefficient for the spectrum region between 0.2 and 20.0 microns and their application to atmospheric optics. *J. Opt. Soc., 47*, 176.

Platt, U., Perner, D. and Patz, H.W. (1979) Simultaneous measurement of atmospheric CH_2O, O_3 and NO_2 by differential optical absorption. *J. Geophys. Res., 84*, C10, 6329-6335.

Platt U., Marquard, L, Wagner, T. and Perner, D. (1997) Corrections for zenith scattered light DOAS. *Geophys. Res. Lett., 24*, 14, 1759-1762.

Pundt, I., Pommereau, J.-P., Goutail F., Chipperfield M.P., Danis, F., Harris N.R.P. and Pyle, J.A. (2000) Vertical distributions of BrO and Bry at high, mid-, and low latitudes. To be in Proc. 5th European Symposium on Stratospheric Ozone Research (Saint-Jean-de-Luz, Basque, France, Sept. 27 September-1 October, 1999).

Richter, A. (1997) Absorptionsspektroskopische Messungen stratosphärischer Spurengase über Bremen, 53°N. Doctoral thesis. The University of Bremen.

Roscoe, H.K., Fish, D.J. and Jones, R.L. (1996) Interpolation errors in UV-visible spectroscopy for stratospheric sensing: implications for sensitivity, spectral resolution, and spectral range. *Appl. Opt., 35,* 427-432.

Roscoe, H.K., Johnston, P.V., Van Roozendael, M., Richter, A., Sarkissian, A., Roscoe, J., Preston, K.E., Lambert, J.-C., Hermans, C., DeCuyper, W., Dzienus, S., Winterrath, T., Burrows, J., Goutail, F., Pommereau, J.-P., D'Almeida, E., Hottier, J., Coureul, C., Didier, R., Pundt, I., Bartlett, L.M., McElroy, C.T., Kerr, J.E., Elokhov, A., Giovanelli, G., Ravegnani, F., Premuda, M., Kostadinov, I., Erle, F., Wagner, T., Pfeilsticker, K., Kenntner, M., Marquard, L.C., Gil, M., Puentedura, O., Arlander, D.W., Kåstad Høiskar, B.A., Tellefsen, C.W., Tørnkvist, K.K., Heese, B., Jones, R.L., Aliwell, S.R., Freshwater, R.A. (1999) Slant column measurement of O_3 and NO_2 during the NDSC intercomparison of zenith-sky UV-visible spectrometers in June 1996. *J. Atmos. Chem., 32*, 281-314.

Rothman, L.S., R.H., Rinsland, A., Goldman, Massie, S.T., Edwards, D.P., Flaud, J.-M., Perrin, A., Camy-Peyret, C., Dana, V., Mandin, J.-Y., Schroeder, J., McCann, A., Gamache, R.R., Wattson, R.B., Yoshino, K., Chance, K.V., Jucks, K.W., Brown, L.R., Nemtchinov, V. and Varanasi, P. (1998) The HITRAN molecular spectroscopic database and HAWKS (HITRAN Atmospheric Workstation): 1996 edition. *J. Quant. Spectrosc. Radiat. Transfer, 60*, 665-710.

Sanders, R.W. (1996) Improved analysis of atmospheric absorption spectra by including the temperature dependence of NO_2. *J. Geophys. Res*, *101*, 20945-20952.

SCUVS-3 (1998) Stratospheric climatology using UV-visible spectroscopy-3. Final report to the Commission of the European Communities. Copenhagen, Danish Meteorological Institute.

Solomon, S., Schmeltekopf, A.L. and Sanders, R.W. (1987) On the interpretation of zenith sky absorption measurements. *J. Geophys. Res., 92*, D7, 8311-8319.

Solomon, S. (1999) Stratospheric ozone depletion: A review of concepts and history. *Rev. Geophys., 37,* 3, 275-316.

Stamnes, K., Tsay, S.-C., Wiscombe, W. and Jayaweera, K. (1988) Numerical stable algorithm for discrete-ordinate-method radiative transfer in multiple scattering and emitting layered media. *Appl. Opt., 27*, 2502-2509.

Tørnkvist, K.K. (2000) Validation of vertical columns of ozone and NO_2 from the SYMOCS instrument. Kjeller, Norwegian Institute for Air Research (NILU TR 2/2000).

United Kingdom Stratospheric Ozone Review Group (1999) Stratospheric ozone 1999. Wetherby, DETR.

Van Roozendael, M., de Mazière and Simon, P. (1994) Ground-based visible measurements at the Jungfraujoch station since 1990. *J. Quant. Spectrosc. Radiat. Transfer, 52*, 231-240.

Vaughan, G., Roscoe, H.K., Bartlett, L.M., O'Connor, F.M., Sarkissian, A., Van Roozendael, M., Lambert, J.-C., Simon, P.C., Karlsen, K., Høiskar, B.A.K., Fish, D.J., Jones, R.L., Freshwater, R.A., Pommereau, J.-P., Goutail, F., Andersen, S.B., Drew, D.G., Hughes, P.A., Moore, D., Mellqvist, J., Hegels, E., Klupfel, T., Erle, F., Pfeilsticker, K., Platt, U. (1997) An intercomparison of ground-based UV-visible sensors of ozone and NO_2. *J. Geophys. Res., 102,* 1411-1422.

Voigt, S., Orphal, J. and Burrows, J.P. (2000) High-resolution reference data by UV-visible Fourier-transform spectroscopy: 2. Absorption cross-sections of O_3 in the 250–800 nm range at atmospheric temperatures (203-293 K). *Chem. Phys. Lett.*, manuscript in preparation.

Wahner, A., Ravishankara, A.R., Sander, S.P. and Friedl, R.R. (1988) Absorption cross-section of BrO between 312 and 385 nm at 298 and 223 K. *Chem. Phys. Lett., 152*, 507-510.

Wahner, A. Tyndall, G.S. and Ravishankara, A.R. (1987) Absorption cross sections for OClO, as a function of temperature in the wavelength range 240-480 nm. *J. Phys. Chem., 91*, 2734-2738.

Wayne, R. (1991) Chemistry of atmospheres. Oxford, Clarendon press.

Appendix A

Airmass factors for ozone, NO_2 and BrO

Table A.1: Airmass factors for ozone, λ=440 nm.

	January	February	March	April	May	June	July	August	September	October	November	December
0.00	0.04	0.12	0.20	0.28	0.37	0.45	0.53	0.62	0.70	0.79	0.87	0.95
30.00	1.04	1.05	1.05	1.06	1.06	1.04	1.04	1.03	1.03	1.03	1.03	1.04
31.00	1.06	1.06	1.06	1.07	1.07	1.05	1.05	1.04	1.04	1.04	1.04	1.05
32.00	1.07	1.07	1.07	1.08	1.08	1.06	1.06	1.05	1.05	1.05	1.05	1.06
33.00	1.08	1.08	1.08	1.09	1.09	1.08	1.07	1.06	1.06	1.06	1.06	1.07
34.00	1.09	1.09	1.09	1.10	1.10	1.09	1.08	1.08	1.08	1.07	1.08	1.08
35.00	1.10	1.10	1.11	1.12	1.11	1.10	1.09	1.09	1.09	1.08	1.09	1.10
36.00	1.12	1.12	1.12	1.13	1.13	1.11	1.11	1.10	1.10	1.10	1.10	1.11
37.00	1.13	1.13	1.13	1.14	1.14	1.13	1.12	1.11	1.12	1.11	1.12	1.12
38.00	1.14	1.15	1.15	1.16	1.16	1.14	1.13	1.13	1.13	1.13	1.13	1.14
39.00	1.16	1.16	1.16	1.17	1.17	1.16	1.15	1.14	1.15	1.14	1.15	1.15
40.00	1.18	1.18	1.18	1.19	1.19	1.17	1.17	1.16	1.16	1.16	1.16	1.17
41.00	1.19	1.19	1.20	1.21	1.20	1.19	1.18	1.18	1.18	1.17	1.18	1.19
42.00	1.21	1.21	1.22	1.22	1.22	1.21	1.20	1.20	1.20	1.19	1.20	1.21
43.00	1.23	1.23	1.23	1.24	1.24	1.23	1.22	1.21	1.21	1.21	1.22	1.23
44.00	1.25	1.25	1.25	1.26	1.26	1.25	1.24	1.23	1.23	1.23	1.24	1.25
45.00	1.27	1.27	1.27	1.28	1.28	1.27	1.26	1.25	1.25	1.25	1.26	1.27
46.00	1.29	1.29	1.30	1.31	1.30	1.29	1.28	1.28	1.28	1.27	1.28	1.29
47.00	1.32	1.32	1.32	1.33	1.33	1.31	1.30	1.30	1.30	1.30	1.30	1.31
48.00	1.34	1.34	1.34	1.35	1.35	1.33	1.33	1.32	1.32	1.32	1.33	1.34
49.00	1.37	1.37	1.37	1.38	1.38	1.36	1.35	1.35	1.35	1.35	1.35	1.36
50.00	1.39	1.39	1.40	1.41	1.40	1.39	1.38	1.37	1.38	1.37	1.38	1.39
51.00	1.42	1.42	1.43	1.43	1.43	1.41	1.41	1.40	1.40	1.40	1.41	1.42
52.00	1.45	1.45	1.46	1.46	1.46	1.44	1.44	1.43	1.43	1.43	1.44	1.45
53.00	1.49	1.49	1.49	1.50	1.49	1.48	1.47	1.46	1.47	1.46	1.47	1.48
54.00	1.52	1.52	1.52	1.53	1.53	1.51	1.50	1.50	1.50	1.50	1.50	1.51
55.00	1.56	1.56	1.56	1.57	1.56	1.54	1.54	1.53	1.54	1.53	1.54	1.55
56.00	1.60	1.59	1.60	1.60	1.60	1.58	1.58	1.57	1.57	1.57	1.58	1.59
57.00	1.64	1.64	1.64	1.65	1.64	1.62	1.62	1.61	1.61	1.61	1.62	1.63
58.00	1.68	1.68	1.68	1.69	1.68	1.67	1.66	1.65	1.66	1.65	1.66	1.67
59.00	1.73	1.73	1.73	1.73	1.73	1.71	1.70	1.70	1.70	1.70	1.71	1.72
60.00	1.78	1.78	1.77	1.78	1.78	1.76	1.75	1.75	1.75	1.75	1.76	1.77
61.00	1.83	1.83	1.83	1.84	1.83	1.81	1.81	1.80	1.80	1.80	1.81	1.82

Table A.1, cont.

	January	February	March	April	May	June	July	August	September	October	November	December
62.00	1.89	1.89	1.88	1.89	1.89	1.87	1.86	1.86	1.86	1.86	1.87	1.88
63.00	1.95	1.95	1.94	1.95	1.95	1.93	1.92	1.92	1.92	1.92	1.93	1.94
64.00	2.01	2.01	2.01	2.02	2.01	1.99	1.99	1.98	1.99	1.98	1.99	2.01
65.00	2.08	2.08	2.08	2.09	2.08	2.06	2.06	2.05	2.06	2.05	2.06	2.08
66.00	2.16	2.16	2.16	2.17	2.15	2.13	2.13	2.13	2.13	2.13	2.14	2.15
67.00	2.24	2.24	2.24	2.25	2.24	2.22	2.21	2.21	2.21	2.21	2.22	2.24
68.00	2.34	2.33	2.33	2.34	2.33	2.30	2.30	2.30	2.30	2.30	2.31	2.33
69.00	2.43	2.43	2.43	2.44	2.42	2.40	2.40	2.39	2.40	2.40	2.41	2.43
70.00	2.54	2.54	2.54	2.54	2.53	2.51	2.50	2.50	2.51	2.50	2.52	2.53
71.00	2.66	2.66	2.65	2.66	2.65	2.62	2.62	2.62	2.62	2.62	2.63	2.65
72.00	2.79	2.79	2.78	2.79	2.77	2.75	2.75	2.74	2.75	2.75	2.76	2.78
73.00	2.94	2.94	2.93	2.93	2.92	2.89	2.89	2.89	2.89	2.89	2.91	2.93
74.00	3.10	3.10	3.09	3.09	3.07	3.05	3.05	3.04	3.05	3.05	3.07	3.09
75.00	3.28	3.28	3.27	3.27	3.25	3.22	3.22	3.22	3.23	3.23	3.25	3.27
76.00	3.49	3.48	3.47	3.47	3.45	3.42	3.42	3.42	3.43	3.43	3.45	3.47
77.00	3.72	3.71	3.70	3.70	3.67	3.64	3.65	3.64	3.66	3.66	3.68	3.71
78.00	3.98	3.98	3.96	3.96	3.93	3.90	3.90	3.90	3.91	3.91	3.94	3.97
79.00	4.29	4.28	4.26	4.26	4.22	4.19	4.19	4.19	4.21	4.21	4.24	4.27
80.00	4.64	4.63	4.61	4.60	4.56	4.53	4.53	4.53	4.55	4.55	4.59	4.62
81.00	5.05	5.04	5.01	5.00	4.96	4.92	4.93	4.93	4.95	4.95	4.99	5.03
82.00	5.54	5.52	5.49	5.48	5.42	5.38	5.39	5.39	5.42	5.43	5.47	5.51
83.00	6.12	6.10	6.06	6.04	5.98	5.93	5.94	5.94	5.97	5.99	6.04	6.09
84.00	6.82	6.80	6.74	6.72	6.64	6.58	6.60	6.61	6.64	6.67	6.72	6.78
85.00	7.68	7.65	7.58	7.54	7.44	7.38	7.40	7.41	7.45	7.49	7.56	7.63
86.00	8.73	8.70	8.61	8.54	8.42	8.34	8.37	8.39	8.45	8.50	8.59	8.68
87.00	10.05	10.01	9.88	9.78	9.62	9.53	9.57	9.60	9.67	9.75	9.87	9.98
88.00	11.72	11.65	11.47	11.31	11.09	10.98	11.05	11.09	11.19	11.31	11.47	11.62
89.00	13.83	13.73	13.46	13.21	12.91	12.78	12.87	12.94	13.09	13.27	13.50	13.70
90.00	16.51	16.36	15.94	15.56	15.14	14.98	15.13	15.25	15.47	15.75	16.07	16.34
91.00	19.59	19.36	18.76	18.24	17.69	17.51	17.75	17.94	18.26	18.66	19.08	19.42

Table A.2: Airmass factors for ozone, λ=510 nm.

	January	February	March	April	May	June	July	August	September	October	November	December
0.00	0.04	0.12	0.20	0.28	0.37	0.45	0.53	0.62	0.70	0.79	0.87	0.95
30.00	1.13	1.13	1.13	1.13	1.13	1.13	1.13	1.13	1.13	1.13	1.13	1.13
31.00	1.14	1.14	1.14	1.14	1.14	1.14	1.14	1.14	1.14	1.14	1.14	1.14
32.00	1.15	1.15	1.15	1.15	1.15	1.15	1.15	1.15	1.15	1.15	1.15	1.15
33.00	1.16	1.16	1.16	1.16	1.16	1.16	1.16	1.16	1.16	1.16	1.16	1.16
34.00	1.17	1.17	1.17	1.17	1.17	1.17	1.17	1.17	1.17	1.17	1.17	1.17
35.00	1.19	1.19	1.19	1.19	1.19	1.18	1.18	1.18	1.18	1.18	1.18	1.19
36.00	1.20	1.20	1.20	1.20	1.20	1.20	1.20	1.20	1.20	1.20	1.20	1.20
37.00	1.21	1.21	1.21	1.21	1.21	1.21	1.21	1.21	1.21	1.21	1.21	1.21
38.00	1.23	1.23	1.23	1.23	1.23	1.23	1.23	1.23	1.23	1.23	1.23	1.23
39.00	1.25	1.25	1.24	1.24	1.24	1.24	1.24	1.24	1.24	1.24	1.24	1.24
40.00	1.26	1.26	1.26	1.26	1.26	1.26	1.26	1.26	1.26	1.26	1.26	1.26
41.00	1.28	1.28	1.28	1.28	1.28	1.27	1.27	1.27	1.27	1.27	1.28	1.28
42.00	1.30	1.30	1.30	1.30	1.29	1.29	1.29	1.29	1.29	1.29	1.29	1.30
43.00	1.32	1.32	1.31	1.31	1.31	1.31	1.31	1.31	1.31	1.31	1.31	1.31
44.00	1.34	1.34	1.33	1.33	1.33	1.33	1.33	1.33	1.33	1.33	1.33	1.33
45.00	1.36	1.36	1.35	1.36	1.35	1.35	1.35	1.35	1.35	1.35	1.35	1.36
46.00	1.38	1.38	1.38	1.38	1.37	1.37	1.37	1.37	1.37	1.37	1.38	1.38
47.00	1.40	1.40	1.40	1.40	1.40	1.39	1.40	1.39	1.40	1.40	1.40	1.40
48.00	1.43	1.43	1.42	1.43	1.42	1.42	1.42	1.42	1.42	1.42	1.42	1.43
49.00	1.45	1.45	1.45	1.45	1.45	1.44	1.44	1.44	1.45	1.45	1.45	1.45
50.00	1.48	1.48	1.48	1.48	1.47	1.47	1.47	1.47	1.47	1.47	1.48	1.48
51.00	1.51	1.51	1.51	1.51	1.50	1.50	1.50	1.50	1.50	1.50	1.50	1.51
52.00	1.54	1.54	1.54	1.54	1.53	1.53	1.53	1.53	1.53	1.53	1.53	1.54
53.00	1.57	1.57	1.57	1.57	1.56	1.56	1.56	1.56	1.56	1.56	1.57	1.57
54.00	1.61	1.61	1.60	1.60	1.60	1.59	1.60	1.60	1.60	1.60	1.60	1.61
55.00	1.64	1.64	1.64	1.64	1.63	1.63	1.63	1.63	1.63	1.63	1.64	1.64
56.00	1.68	1.68	1.68	1.68	1.67	1.67	1.67	1.67	1.67	1.67	1.68	1.68
57.00	1.72	1.72	1.72	1.72	1.71	1.71	1.71	1.71	1.71	1.71	1.72	1.72
58.00	1.77	1.77	1.76	1.76	1.76	1.75	1.75	1.75	1.76	1.76	1.76	1.77
59.00	1.81	1.81	1.81	1.81	1.80	1.80	1.80	1.80	1.80	1.80	1.81	1.81
60.00	1.86	1.86	1.86	1.86	1.85	1.85	1.85	1.85	1.85	1.85	1.86	1.86
61.00	1.92	1.92	1.91	1.91	1.90	1.90	1.90	1.90	1.90	1.90	1.91	1.92

Table A.2, cont.

	January	February	March	April	May	June	July	August	September	October	November	December
62.00	1.98	1.97	1.97	1.97	1.96	1.96	1.96	1.96	1.96	1.96	1.97	1.97
63.00	2.04	2.04	2.03	2.03	2.02	2.02	2.02	2.02	2.02	2.02	2.03	2.03
64.00	2.10	2.10	2.10	2.10	2.09	2.08	2.08	2.08	2.09	2.09	2.09	2.10
65.00	2.18	2.17	2.17	2.17	2.16	2.15	2.15	2.15	2.16	2.16	2.16	2.17
66.00	2.25	2.25	2.24	2.24	2.23	2.23	2.23	2.23	2.23	2.23	2.24	2.25
67.00	2.34	2.34	2.33	2.33	2.32	2.31	2.31	2.31	2.32	2.32	2.33	2.33
68.00	2.43	2.43	2.42	2.42	2.41	2.40	2.40	2.40	2.41	2.41	2.42	2.43
69.00	2.53	2.53	2.52	2.52	2.51	2.50	2.50	2.50	2.51	2.51	2.52	2.53
70.00	2.64	2.64	2.63	2.63	2.61	2.60	2.61	2.61	2.62	2.62	2.63	2.64
71.00	2.76	2.76	2.75	2.75	2.73	2.72	2.73	2.73	2.74	2.74	2.75	2.76
72.00	2.90	2.89	2.88	2.88	2.87	2.85	2.86	2.86	2.87	2.87	2.88	2.89
73.00	3.04	3.04	3.03	3.03	3.01	3.00	3.00	3.00	3.01	3.01	3.03	3.04
74.00	3.21	3.21	3.19	3.19	3.17	3.16	3.17	3.17	3.18	3.18	3.19	3.20
75.00	3.40	3.39	3.38	3.37	3.35	3.34	3.35	3.35	3.36	3.36	3.37	3.39
76.00	3.61	3.60	3.59	3.58	3.56	3.54	3.55	3.55	3.56	3.57	3.58	3.60
77.00	3.85	3.84	3.82	3.82	3.79	3.77	3.78	3.78	3.80	3.80	3.82	3.84
78.00	4.12	4.11	4.09	4.08	4.06	4.04	4.05	4.05	4.06	4.07	4.09	4.11
79.00	4.43	4.42	4.40	4.39	4.36	4.34	4.35	4.35	4.37	4.37	4.40	4.42
80.00	4.80	4.79	4.76	4.75	4.72	4.69	4.71	4.71	4.72	4.73	4.76	4.78
81.00	5.23	5.22	5.19	5.17	5.14	5.11	5.12	5.12	5.14	5.15	5.18	5.21
82.00	5.74	5.72	5.69	5.67	5.63	5.60	5.61	5.62	5.64	5.65	5.69	5.72
83.00	6.35	6.33	6.29	6.27	6.22	6.18	6.20	6.20	6.23	6.25	6.29	6.33
84.00	7.10	7.08	7.03	6.99	6.93	6.89	6.91	6.92	6.94	6.97	7.02	7.07
85.00	8.02	7.99	7.92	7.88	7.80	7.75	7.77	7.78	7.82	7.86	7.92	7.97
86.00	9.16	9.12	9.04	8.97	8.88	8.82	8.84	8.85	8.89	8.96	9.03	9.10
87.00	10.59	10.53	10.43	10.33	10.22	10.14	10.15	10.18	10.23	10.32	10.42	10.51
88.00	12.39	12.31	12.17	12.02	11.87	11.77	11.79	11.83	11.89	12.03	12.15	12.27
89.00	14.65	14.54	14.33	14.10	13.90	13.78	13.80	13.86	13.94	14.15	14.32	14.48
90.00	17.52	17.36	17.04	16.69	16.41	16.24	16.27	16.37	16.49	16.81	17.05	17.27
91.00	21.00	20.76	20.28	19.75	19.35	19.15	19.22	19.37	19.55	20.03	20.38	20.67

Table A.3: Airmass factors for NO_2.

SZA	AMF	SZA	AMF
30	1.14	64	2.16
31	1.15	65	2.23
32	1.17	66	2.31
33	1.18	67	2.4
34	1.19	68	2.5
35	1.2	69	2.6
36	1.22	70	2.71
37	1.23	71	2.84
38	1.25	72	2.98
39	1.26	73	3.13
40	1.28	74	3.3
41	1.3	75	3.49
42	1.32	76	3.7
43	1.34	77	3.94
44	1.36	78	4.22
45	1.38	79	4.53
46	1.4	80	4.9
47	1.43	81	5.32
48	1.45	82	5.82
49	1.48	83	6.42
50	1.51	84	7.14
51	1.54	85	8.01
52	1.57	86	9.08
53	1.61	87	10.41
54	1.64	88	12.09
55	1.68	89	14.24
56	1.72	90	17.04
57	1.76	91	20.53
58	1.81	92	24.53
59	1.86	93	28.21
60	1.91	94	30.05
61	1.96	95	30.62
62	2.02	96	34.93
63	2.09		

Table A.4: Airmass factors for BrO.

SZA	AMF	SZA	AMF
20.00	1.26	58.00	2.12
21.00	1.27	59.00	2.18
22.00	1.28	60.00	2.23
23.00	1.29	61.00	2.30
24.00	1.30	62.00	2.36
25.00	1.31	63.00	2.43
26.00	1.32	64.00	2.50
27.00	1.33	65.00	2.58
28.00	1.34	66.00	2.67
29.00	1.35	67.00	2.76
30.00	1.36	68.00	2.87
31.00	1.38	69.00	2.98
32.00	1.39	70.00	3.10
33.00	1.40	71.00	3.23
34.00	1.42	72.00	3.37
35.00	1.44	73.00	3.53
36.00	1.45	74.00	3.71
37.00	1.47	75.00	3.90
38.00	1.49	76.00	4.12
39.00	1.51	77.00	4.37
40.00	1.53	78.00	4.65
41.00	1.55	79.00	4.97
42.00	1.57	80.00	5.33
43.00	1.59	81.00	5.75
44.00	1.62	82.00	6.25
45.00	1.64	83.00	6.83
46.00	1.67	84.00	7.51
47.00	1.70	85.00	8.33
48.00	1.73	86.00	9.31
49.00	1.76	87.00	10.50
50.00	1.79	88.00	11.90
51.00	1.82	89.00	13.40
52.00	1.86	90.00	15.00
53.00	1.90	91.00	16.60
54.00	1.94	92.00	17.00
55.00	1.98	93.00	16.50
56.00	2.03	94.00	15.80
57.00	2.07	95.00	15.00

Norwegian Institute for Air Research (NILU)
P.O. Box 100, N-2027 Kjeller, Norway

REPORT SERIES TECHNICAL REPORT	REPORT NO. TR 1/2000	ISBN 82-425-1150-0 ISSN 0807-7185	
DATE	SIGN.	NO. OF PAGES 74	PRICE NOK 200.-

TITLE The development of the SYMOCS instruments and the spectral analysis	PROJECT LEADER Kjersti K. Tørnkvist
	NILU PROJECT NO. U-95091/U-98009
AUTHOR(S) Kjersti K. Tørnkvist	CLASSIFICATION * A
	CONTRACT REF.

REPORT PREPARED FOR
Norwegian Institute for Air Research
P.O. Box 100
N-2027 Kjeller
Norway

ABSTRACT

Since 1995, Norwegian Institute for Air Research (NILU) has measured the stratospheric compounds O_3, NO_2, BrO and OClO with a ground-based spectrometer that measures the scattered light from the zenith sky. The instrument system called SYMOCS (SYstem for MOnitoring Compounds in the Stratosphere), was developed at NILU. During 1998 a similar spectrometer system was developed in order to optimise the measurements of the four compounds. The two instrument systems are called SYMOCS-VIS (O_3 and NO_2) and SYMOCS-UV (BrO and OClO). This report describes the development and characterisation of the two instruments as well as the spectral analysis and retrieval of the compounds.

NORWEGIAN TITLE

Utvikling av SYMOCS-instrumentene og den spektrale analyse.

KEYWORDS		
UV-visible spectrometer	DOAS spectral analysis	Slant columns/vertical columns

ABSTRACT (in Norwegian)

Siden 1995 har NILU målt O_3, NO_2, BrO og OClO i stratosfæren med et bakkebasert spektrometer som måler spredt lys fra zenit. Instrumentet som ble kalt SYMOCS (SYstem for MOnitoring Compounds in the Stratosphere), ble utviklet ved NILU. I 1998 ble et tilsvarende spektrometer-system utviklet for å optimalisere målingene av de fire stratosfæriske komponentene. De to systemene kalles nå SYMOCS-VIS (O_3 og NO_2) og SYMOCS-UV (BrO og OClO). Denne rapporten beskriver utvikling og karakterisering av de to instrumentene sammen med den spektrale analyse og beregning av komponentene.

** Classification* *A* *Unclassified (can be ordered from NILU)*
B *Restricted distribution*
C *Classified (not to be distributed)*